

Novel Quantum Spin Hall Effect in SmB_6 - a Strong Topological Insulator

**Partha Goswami and Udai Prakash Tyagi*

D.B.College, University of Delhi, Kalkaji, New Delhi-110019, India

**Email of the corresponding author: physicsgoswami@gmail.com*

Email of the second author: uptyagi@yahoo.co.in

Abstract In this communication we show analytically that the compound samarium hexaboride SmB_6 is a strong topological Kondo insulator. We consider the periodic Anderson model in the long wavelength limit. The Anderson Hamiltonian is written down in the Dirac basis in a form similar to the Bernevig–Hughes–Zhang model presented over a decade and half ago for quantum wells. Thereafter, we obtain the Z_2 invariant using the eigenvalues of the space inversion operator in the Fu-Kane framework. We also show novel quantum spin Hall state with broken time reversal symmetry due to the normal incidence of circularly polarized optical field on the surface of SmB_6 using the Floquet theory.

1.Introduction

The recipe required for the formation of the topologically non-trivial surface states in a generic topological Kondo Insulator (GTKI)[1-3] are band inversion by hybridization and strong spin-orbit coupling. The latter does not break the time reversal symmetry (TRS). The strong correlation effects and diverse surface conditions make the system extremely complicated. This communication is on a topical issue of the mixed valence compound SmB_6 .—a narrow gap topological Kondo insulator (TKI) which, with a high-temperature metallic phase, transforms into a paramagnetic charge insulator below 45 K. These are a particular class of strongly-interacting heavy-fermion materials. The strong correlation effects and diverse surface conditions make the system extremely complicated and almost a Gordian knot. The origin of the itinerant electron Fermi surface (FS), originating from the in-gap states, is still a mystery. Quite a few works related to its peculiarities are discussed in section 5. It has been suggested [1,2], as well as there is mounting evidence [4-6] during the past several years, that SmB_6 is a strong topological insulator. This has generated great deal of excitement in the condensed matter physics community and it still remains a matter of intense debate [7]. The supporting evidence for the TKI scenario [4-6] notwithstanding, there is no jury-verdict regarding the nature of the bulk and surface states of SmB_6 [7-9]. In this communication we show conclusively that the SmB_6 surface state is topologically non-trivial as the material band structure features odd numbers of pair intersections at time reversal invariant momenta (TRIMs). The moderate disorder cannot remove such pair-surface-state crossings (SSCs) which correspond to the topological index $Z_2 = -1$ ($\nu_0 = 1$). We consider extension of the slave boson (SB) mean-field-theoretic version of the periodic Anderson model (PAM) [3, 10-12] for a generic topological Kondo insulator (GTKI) on a simple cubic lattice with one spin-degenerate orbital per lattice site each for d and f electrons for this purpose. The PAM Hamiltonian is written down in the Dirac basis similar to the Bernevig–Hughes–Zhang

(BHZ) model presented over a decade and half ago for quantum wells. Thereafter, we obtain the Z_2 invariant using the eigenvalues of the space inversion operator in the Fu-Kane framework [13].

The polarized periodic optical field provides a potent modus operandi to carry out theoretical proposition and experimental realization, manipulation, and detection of diverse unconventional/novel optical and electronic properties of materials, such as the polarization-dependent optoelectronic device applications in 2D materials and their heterostructures [11,12], the realization of novel quantum phases without static counterparts like light induced quantum anomalous phase (QAH) phase [14], the topological phase transitions in semi-metals [15-20], the Floquet engineering of magnetism in topological insulator thin films [21,22], and so on. The exotic Floquet topological phases with a high tunability could be realized using this highly efficient and promising platform by band-structure engineering. In fact, there has been an upsurge on experimental front in the search for topological states, in solid state [23], cold-atom [24] and optical systems [25], which are driven periodically. The circularly polarized optical field (CPOF) is described by a time-periodic (time period = $T = 2\pi/\omega$ where ω is the frequency of light) gauge field. Upon using the Peierls substitution, lattice electrons couple to the electromagnetic gauge field. In the presence of COPF, the thin film Hamiltonian $H_{surface}$, apart from breaking the time reversal invariance (TRS), becomes periodic in time. One can now transform the time-dependent Hamiltonian problem to a time-independent one using the Floquet's theorem [26-29]. Analogous to the Bloch theory, a solution for the time-dependent Schrodinger equation of the system is obtained here involving the Floquet quasi-energy and the time-periodic Floquet state with the periodicity T . The Floquet state could be expanded in a Fourier series which makes us arrive at an infinite dimensional eigenvalue equation in the Sarnbe space [26]. The circularly polarized light incident upon the film may be described by a time-varying gauge field $\mathbf{A}(t)$. Once we have included a gauge field, it is necessary that we make the Peierls substitution $H_{surface}(t) = H_{surface}\left(\mathbf{k} - \frac{e}{\hbar}\mathbf{A}(t)\right)$. In view of the Floquet theory [26-29], in the high-frequency limit, our thin film system, irradiated by the circularly polarized radiation, can be described by an effective, static Hamiltonian. We make use of the Floquet theory in section 4, in the high-frequency limit, to investigate the system. Interestingly, the optical field leads to the emergence of quantum spin Hall (QSH) phase even when the time reversal symmetry (TRS) is broken.

Our minimalistic bulk Hamiltonian captures essential physics of GTKI in the presence of the coulomb repulsion U_f ($\gg t_{d1}$) between f electrons on the same site, and the spin-orbit hybridization V . The terms (t_{d1}, t_{f1}) are the NN hopping parameter for d and f electrons. The band warping factor, usually associated with the Hamiltonian of a topological insulator, has not been considered here for the mathematical simplicity. There are three parameters (b, λ, ξ) of the SB theory [3]. The method to obtain them is explained clearly in ref. [3]. We never-the-less summarize briefly below to make this paper self-contained. The constraint $U_f \gg t_{d1}$ imposes a non-holonomic constraint, viz. the exclusion of the double occupancy, which is very difficult to manipulate. The SB- framework provides a platform to reformulate this nonholonomic constraint

into a holonomic constraint that can be implemented with a Lagrange multiplier. Here, an electron annihilation operator is written as the product of a spinless boson creation operator (SB) and a spinful fermion annihilation operator (We represent them by annihilation operators $f_{k,\tau}^\dagger = (b^\dagger c_{k,\tau})$ in momentum space. Here, the index τ ($= \uparrow, \downarrow$) represents the spin.). This basically corresponds to the assumption that the annihilation of an electron is equivalent to simultaneous creation of a slave-bosonic hole and annihilation of a fermionic spinon. In the present SB framework, we make the further assumption that the slave boson field (b) at each lattice site can be replaced by a c -number. The complications associated with the large on-site repulsion ($U_f \gg t_{d1}$) between the f -electrons is conveniently circumvented in the SB theory by imposing the holonomic constraint $\sum_\tau (c_\tau^\dagger c_\tau) = 1 - b^2$ at a site to remove the double occupancy. The term $\lambda [\sum_{k,\tau = \uparrow, \downarrow} (c_{k,\tau}^\dagger c_{k,\tau}) + N_c (b^2 - 1)]$, where N_c (N_d) is the number of c -fermions (d -fermions) and $N_c = N_d$ required for the formation of Kondo singlet states between d and c fermions at each lattice site, to be added to the system Hamiltonian to enforce the constraint on the pseudo-particles due to the infinite on-site Coulomb repulsion. Therefore, the signature of the assumption “large on-site repulsion ($U_f \gg t_{d1}$) between the f -electrons” is carried over by the parameters λ and b . The constant term $\lambda N_c (b^2 - 1)$ in the Hamiltonian (1) is to be dropped here-in-after as it has no significance in the calculation below. Moreover, we neglected the dynamics of the boson field completely as the light slave boson creation and destruction operators were replaced by a c -number ‘ b ’. This approximation reduced the system to a non-interacting one with the bulk spectral gap dependent on the parameters (b, λ, ξ, V). Whereas the first two parameters took care of the strong correlation effect between the f -electrons, the hybridization parameter V is the harbinger of a topological dispensation. The term ξ enforces the fact that there are equal number of d and f fermions. In order to have a Kondo insulator, formation of singlet states between d and f fermions is needed at each lattice site. This means that the number of d and f fermions are equal on average. The total parameters are slave-boson field b , auxiliary chemical potentials ζ and μ (μ is a free parameter), and the Lagrange multiplier λ . One obtains equations for the parameters (b, λ, ξ) minimizing the thermodynamic potential per unit volume. We find that $\lambda = -6t_{f1} + 6b^2t_{f1}$, and $\xi = -3t_{d1} + 3t_{f1}$. The admissible value of b^2 is 1^- .

The paper is organized as follows: In section 2, we obtain the surface state band spectrum in slave-boson formalism. We show that the surface state Hamiltonian corresponds to Qi-Wu-Zhang (QWZ) model[30-33] in the absence of the magnetic impurities. As shown by these authors, the situation corresponds to QSH state. In section 3, we calculate Z_2 invariant using the eigenvalues of the space inversion operator with in the Fu-Kane framework [13]. In section 4, we are able to show fledgling QSH phase by the normal incidence of tunable CPOF, even when the TRS is broken. For this purpose, we start with a low-energy two-dimensional, time-dependent Hamiltonian. The time dependence arises due to CPOF describable by the associated gauge field. We make use of the Floquet theory in the high-frequency limit to investigate the system. The TKI has a bulk gap due to hybridization between localized and conduction electrons. A mystery centers on the existence of the bulk in-gap states and why they appear in some situations but not others.

For example, quantum oscillations in SmB₆ appear in magnetization but not in resistivity, the lack of electrical transport signature in epitaxial thin films in contrast with that in bulk, etc.. We point out these issues and related ones as well in section 5 together with very brief concluding remarks.

2. Surface State Band Spectrum in slave-boson formalism

We consider below extension of the slave boson (SB) mean-field-theoretic version of the periodic Anderson model (PAM) [3,10-12, 34,35] for a (topological) Kondo insulator on a simple cubic lattice with one spin-degenerate orbital per lattice site each for d and f electrons. The SB protocol has been summarized below. In momentum(\mathbf{k})-space, we represent them by creation (annihilation) operators $d_{\mathbf{k},\tau}^\dagger$ ($d_{\mathbf{k},\tau}$) and $f_{\mathbf{k},\tau}^\dagger = b c_{\mathbf{k},\tau}^\dagger$ ($b c_{\mathbf{k},\tau}$), respectively. Here, the index τ ($= \uparrow, \downarrow$) represents the spin. The Hamiltonian H_{PAM} consists of three parts, namely, the hopping of the individual orbitals, the hybridization parameter V between d and f orbitals, and an onsite repulsion of f electrons (\mathfrak{N}_{int}). The exchange energy M due to magnetic impurities will be added later. The Hamiltonian in ref.[3] with a cavalcade of ingredients on a simple cubic lattice in momentum-space is as follows:

$$H_{PAM}(b, \lambda, \xi) = \sum_{\mathbf{k}, \tau = \uparrow, \downarrow} \widetilde{E}_k^d(\mu, \xi) d_{\mathbf{k}, \tau}^\dagger d_{\mathbf{k}, \tau} + \sum_{\mathbf{k}, \tau = \uparrow, \downarrow} \widetilde{E}_k^f(\mu, b, \lambda, \xi) c_{\mathbf{k}, \tau}^\dagger c_{\mathbf{k}, \tau} + b \sum_{\mathbf{k}, \tau = \uparrow, \downarrow} \{F_{\tau = \uparrow, \downarrow}(k) \langle d_{\mathbf{k}, \tau}^\dagger c_{\mathbf{k}, \tau} \rangle + \text{H.C.}\} + \lambda N_c (b^2 - 1) + \mathfrak{N}_{int} \quad (1)$$

$$\widetilde{E}_k^d(\mu, \xi) = -\mu - \xi - [2t_{d1} c_1(k) + 4t_{d2} c_2(k) + 8t_{d3} c_3(k)], \mathbf{k} = (k_x, k_y) \quad (2)$$

$$\widetilde{E}_k^f(\mu, b, \lambda, \xi) = -\mu + \xi - b^2 [-\epsilon_f + 2t_{f1} c_1(k) + 4t_{f2} c_2(k) + 8t_{f3} c_3(k)] + \lambda, \quad (3)$$

$$c_1(k) = (\cos k_x a + \cos k_y a + \cos k_z a), \quad (4)$$

$$c_2(k) = (\cos k_x a \cdot \cos k_y a + \cos k_y a \cdot \cos k_z a + \cos k_z a \cdot \cos k_x a), \quad (5)$$

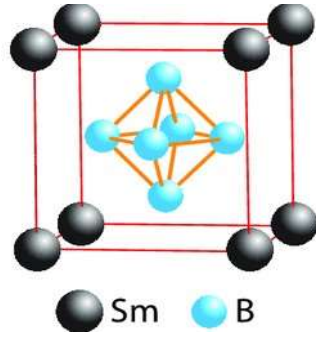
$$c_3(k) = (\cos k_x a \cdot \cos k_y a \cdot \cos k_z a), \quad (6)$$

$$\mathfrak{N}_{int} = U_f \sum_{i(\text{site index})} f_{i\uparrow}^\dagger f_{i\uparrow} f_{i\downarrow}^\dagger f_{i\downarrow}. \quad (7)$$

As one can see from (1), the dispersion of the f -electron is renormalized by λ and its hopping amplitude by b^2 . Moreover, the hybridization amplitude is also renormalized by the c -number b . Since the f - and d -states have different parities, the momentum-dependent form-factor matrix $F_{\tau = \uparrow, \downarrow}(k)$ involved in the third term in (1) must be odd: $F_{\tau = \uparrow, \downarrow}(-k) = -F_{\tau = \uparrow, \downarrow}(k)$. This is required in order to preserve time reversal symmetry (TRS), as the matrix involves coupling with the physical spin of the electron. Therefore, we write $F_{\tau = \uparrow, \downarrow}(k) = 2V(\mathbf{s}(k) \cdot \boldsymbol{\tau}')$, where V is a constant parameter characterizing the spin-orbit hybridization, $\mathbf{s}(k) = (\sin k_x a, \sin k_y a, \sin k_z a)$ and $\boldsymbol{\tau}' =$

(τ_x, τ_y, τ_0) are the Pauli matrices in spin space. The terms (t_{d1}, t_{f1}) , (t_{d2}, t_{f2}) , and (t_{d3}, t_{f3}) , respectively, are the NN , NNN , and $NNNN$ hopping parameters for d and f electrons; ϵ_f is the onsite energy of the f electrons and N_c is the number of lattice sites for these electrons.

In Figure 1(a), we have shown a diagrammatic representation of SmB_6 crystal structure with cubic lattice constant $a = 0.413$ nm. The Sm ions are located at the corners and the B_6 octahedron at the center of the cubic lattice. In Figure (b) and (c), we have plotted the bulk band energies (eigenvalues of (1)) of the present TKI system in the insulating phase (where t_{f1} is negative) assuming the quasi-particles non-interacting; the spin-orbit hybridization is included in Figure 1(c). The system shows the bulk metallic as well as the bulk insulating phases determined by the



(a)

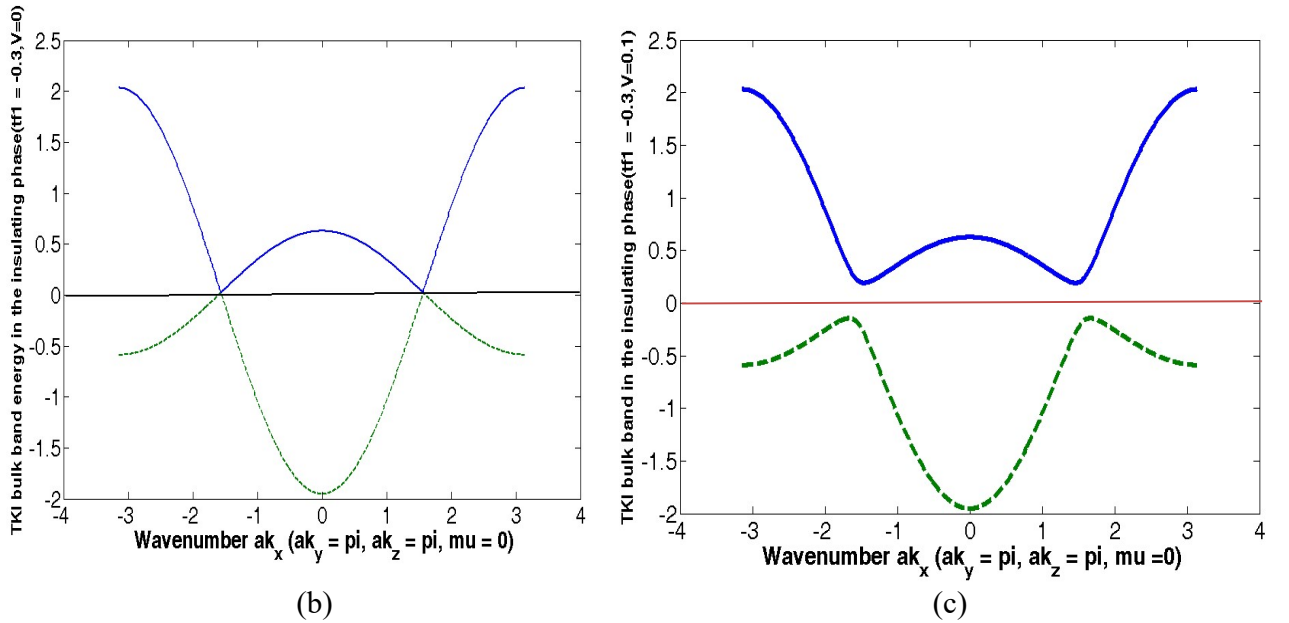


Figure 1. (a) A diagrammatic representation of SmB_6 crystal structure with cubic lattice constant $a = 0.413$ nm. The Sm ions are located at the corners and the B_6 octahedron at the center of the cubic lattice. (b), (c) The plots of

the bulk band energies (eigenvalues of Eq. (1)) of the present TKI system in the insulating phase assuming the quasi-particles non-interacting. The hybridization parameter V is zero in (b), whereas it is 0.1 in (c). The latter one represents an insulating bulk. The numerical values of the parameters used in the plots are $t_{d_1} = 1$, $t_{f_1} = -0.3$, $t_{d_2} = 0.01$, $t_{f_2} = 0.01$, $t_{d_3} = 0.001$, $t_{f_3} = 0.001$, $\epsilon_f = -0.02$, $V = (0, 0.1)$, $b = 0.98$, $\mu = 0$, and $U_f \gg t_{d_1}$.

sign of t_{f_1} . It is positive for the former and negative for the latter phase [3]. The negative sign of t_{f_1} is also necessary for the band inversion, which induces the topological state [3]. Throughout the paper, we choose t_{d_1} to be the unit of energy. The numerical values of the parameters used in the plots are $t_{d_1} = 1$, $t_{f_1} = -0.3$ (negative value ensures insulating bulk), $t_{d_2} = 0.01$, $t_{f_2} = 0.01$, $t_{d_3} = 0.001$, $t_{f_3} = 0.001$, $\epsilon_f = -0.02$, $V = (0, 0.1)$, $b = 0.98$, $\mu = 0$, and $U_f = 0$. Here since the coulomb repulsion U_f between f electrons on the same site is taken into account, the correlation effect is not missing. We do find that $V = 0$ ($V \neq 0$) case does correspond to band crossing (avoided crossing) - an essential feature of SmB_6 . All energies in our calculation/ graphical representation below are expressed in units of the first neighbor hopping t_{d_1} for d-electrons as this corresponds to the kinetic energy of these itinerant electrons and therefore the most dominant.

We shall treat the model Hamiltonian (1) in the long wave-length limit below. In the above limit, the following replacements are necessary: $\sin(a_j k_j) \rightarrow a_j k_j + O(a_j^3 k_j^3)$ and $\cos(a_j k_j) \rightarrow (1 - \frac{1}{2} a_j^2 k_j^2) + O(a_j^4 k_j^4)$ where $j = (x, y, z)$, and a_j is the lattice constant along j direction. Furthermore, in order to obtain surface state Hamiltonian ($H_{\text{surface}}(k, \lambda, \mu, \xi, b)$) we make the replacement $ak_z \rightarrow -ia \partial_z$ and look for states localized within the surface $z = 0$ of the form $\exp(-i\chi z)$. Furthermore, we seek such a value of the unknown wave number χ ($\chi = -iq, q > 0$) for which the exponential $\exp\left(-\frac{aqz}{a}\right) \ll 1$ for $z > 0$. For example, if we assume $aq \sim 1$ the exponential $\exp\left(-\frac{aqz}{a}\right) \sim \exp(-10)$, i.e vanishingly small, for $z \sim 50 \text{ nm}$ given that SmB_6 crystal structure with cubic lattice constant $a = 0.413 \text{ nm}$ (Figure 1(a)). Therefore, $\chi = -iq, q > 0$ ensures a decaying term for $z > 0$ in the surface states. For $z < 0$, the exponential will be $\exp\left(\frac{aq|z|}{a}\right)$. This implies that, in SmB_6 , the surface state possesses much greater penetration depth unlike that in Bi_2Se_3 (the penetration depth $\sim 5\text{-}10 \text{ nm}$). This seems to be an extraordinary feature which offers a possible reconciliation of the lack of electrical transport signature in epitaxial thin films in contrast with that in bulk.

We intend to take ferromagnetic magnetic impurities (FMI) doped in SmB_6 into consideration. We model the required interaction between an alien MI moment and the electrons in the system with coupling term ($J \sum_m S_m \cdot s_m$), where S_m is the m th-site impurity spin, $s_m = \sum_{\tau} \left(\frac{1}{2}\right) o_{m,\tau}^{\dagger} \tau_z o_{m,\tau}$, $o_{m,\tau}$ is the electron annihilation operator at site- m and spin-state τ ($=\uparrow, \downarrow$) and τ_z is the z -component of the Pauli matrices. We make the approximation of treating the impurity spins as classical vectors. The latter is valid for $|\mathbf{S}| > 1$. We absorb the magnitude of the impurity spin into the ferromagnetic coupling constant J and write $M = |J| |\mathbf{S}|$. Upon including the RSOC, RDP, and the exchange coupling M , in the basis $(d_{k,\uparrow}^{\dagger} \ bc_{k,\downarrow}^{\dagger} \ d_{k,\downarrow}^{\dagger} \ bc_{k,\uparrow}^{\dagger})^{\text{T}}$, from above we find

$$h_{\text{surface}}(k, \chi, \mu, b, M) = (\epsilon(k, \chi, \mu, b))\sigma_0 \otimes \tau_0 + A_1 a k_x \sigma_z \otimes \tau_x + A_1 a k_y \sigma_z \otimes \tau_y + \vartheta(k, b, \chi) \sigma_0 \otimes \tau_z + M \sigma_z \otimes \tau_z + \left(\frac{1}{2}\right) [-i A_1 a q (\sigma_x + i \sigma_y) \otimes \tau_x + i A_1 a q (\sigma_x - i \sigma_y) \otimes \tau_x] \quad (8)$$

Here $\sigma_{x,y,z}$ are also the Pauli matrices, σ_0 is the 2×2 identity matrix. The term $\left[\left(\frac{1}{2}\right) (\Delta - \alpha_0 \sin(k_y a)) \sigma_x \otimes (\tau_z + \tau_0) + \left(\frac{1}{2}\right) \alpha_0 \sin(k_x a) \sigma_y \otimes (\tau_z + \tau_0)\right]$ is the Rashba spin-orbit coupling (RSOC) between the d -electrons. This is to be considered briefly in the discussion to examine how the broken inversion symmetry affect our result. As there is evidence of for a massive surface state at the surface Brillouin zone center which can exhibit Rashba splitting [64], it would be interesting to see how does surface state react to RSOC and the term Δ is expected to yield the splitting at the Γ point. All the functions appearing in Eq. (8) are given in Appendix A (see Eq.(A.1)). Upon dropping the last term in (8), we find that the Hamiltonian (8), in the basis $(d_{\mathbf{k},\uparrow}^\dagger, bc_{\mathbf{k},\downarrow}^\dagger, d_{\mathbf{k},\downarrow}^\dagger, bc_{\mathbf{k},\uparrow}^\dagger)^\top$, could be written as

$$h_{\text{surface}}(k, q, \mu, b, M) = (\epsilon(k, q, \mu, b))\sigma_0 \otimes \tau_0 + \vartheta(k, q, b)\sigma_0 \otimes \tau_z + A_1 a k_x \sigma_z \otimes \tau_x + A_1 a k_y \sigma_z \otimes \tau_y + M \sigma_z \otimes \tau_z \quad (9)$$

$$h_{\text{surface}}(k, q, \mu, b, M) = \begin{pmatrix} \mathfrak{h}_+ = \mathfrak{h}(k_x, k_y, q, \mu, b, M) & 0 \\ 0 & \mathfrak{h}_- = \mathfrak{h}^*(-k_x, -k_y, q, \mu, b, -M) \end{pmatrix} \quad (10)$$

where $\mathfrak{h}_+ = (\epsilon(k, q, \mu, b))\tau_0 + \mathbf{n}(k_x, k_y, q, b) \cdot \boldsymbol{\tau} + M \tau_z$, the two blocks (\mathfrak{h}_+ , \mathfrak{h}_-), characterized by the pseudo-spin indices (+, -), are related to each other by time reversal symmetry (TRS) for $M = 0$, and $\mathbf{n}(k_x, k_y, q, b) = (A_1 a k_x, A_1 a k_y, \vartheta(k_x, k_y, q, b))$. On a quick side note, it is worth mentioning that $h_{\text{surface}}(k, q, \mu, b, M = 0)$ corresponds to Qi-Wu-Zhang (QWZ) model[30-33]. As shown by these authors, the situation corresponds to the QSH state, for the spin Hall conductance of $\mathfrak{h}(k_x, k_y, q, \mu, b, M = 0)$ and $\mathfrak{h}^*(-k_x, -k_y, q, \mu, b, -M = 0)$ are not zero but the net Hall conductance of the system described by Eq.(10) is zero. The quantum spin Hall (QSH) effect is a spin version of quantum Hall effect associated with the locking of the surface electron spin perpendicularly to the Bloch \mathbf{k} -vector. A trivial insulator has gapped edge, while a quantum spin Hall one has a pair of gapless helical edge states carrying opposite spins. Moreover, a twisted Hilbert space is the important feature of a QSH system (or a strong topological insulator). We show below that the Hilbert space of our system is twisted. The appearance of topologically-protected surface states is the physical consequence of this nontriviality.

3. Z_2 Invariant using the Eigenvalues of the Space Inversion Operator

For the purpose stated above, following Fu and Kane [13], the Z_2 invariant using the eigenvalues of the parity operator needs to be calculated. The objective could be accomplished with relative ease if the Hamiltonian in (8) is written down in the Dirac basis similar to the Bernevig–Hughes–

Zhang (BHZ) model [30] presented over a decade and half ago for quantum wells. We write the Hamiltonian in (8) as

$$h_{\text{surface}} = \begin{pmatrix} \mathfrak{b}_+ & \mathcal{L}_1 \\ \mathcal{L}_2 & \mathfrak{b}_- \end{pmatrix}, \quad \mathcal{L}_1 = \begin{pmatrix} 0 & -iA_1aq \\ -iA_1aq & 0 \end{pmatrix}, \quad \mathcal{L}_2 = \begin{pmatrix} 0 & iA_1aq \\ iA_1aq & 0 \end{pmatrix}, \quad (11)$$

where $ak_{\mp} = ak_x \mp iak_y$. The interblock coupling is incorporated by the matrices ($\mathcal{L}_1, \mathcal{L}_2 = \mathcal{L}_1^\dagger$). All features of a physical system reside in the properties of the corresponding Hamiltonian. The Hamiltonian (12) is Hermitian and hence eigenvalues are real. For complex eigenvalues, the Hamiltonian eigenfunctions are not eigenfunctions of the parity-time reversal transformation PT operator [72], i.e. $[H, PT] \neq 0$. It must be noted that P is a linear unitary operator, T is an antilinear and antiunitary operator and hence PT is also antilinear and antiunitary. We now write the Hamiltonian in (11) in Dirac basis similar to the BHZ model: In terms of the column vector $(d_{k,\uparrow}^\dagger, d_{k,\downarrow}^\dagger, bc_{k,\uparrow}^\dagger, bc_{k,\downarrow}^\dagger)^\top$, we have

$$h_{\text{surface}}^{\text{BHZ}}(k, q, \mu, b, M) = \frac{\epsilon_d + \epsilon_c}{2} I^{4 \times 4} + \sum_{a=0,1,2,3,5} d_a(k, q, \mu, b) \gamma^a + M \sigma_0 \otimes \tau_z \quad (12)$$

where $d_0 = \frac{\epsilon_d - \epsilon_c}{2}$, $\epsilon_d = (\epsilon(k, q, \mu, b) + \vartheta(k, q, b))$, $\epsilon_c = (\epsilon(k, q, \mu, b) - \vartheta(k, q, b))$, $d_1 = -iA_1ak_y$, $d_2 = iA_1ak_x$, $d_3 = A_1a\chi$, and $d_5 = 0$. The Hamiltonian $h_{\text{surface}}^{\text{BHZ}}(k, q, \mu, b, M = 0)$ corresponds to the periodic Anderson Hamiltonian (PAM) in the long wavelength limit for the special case $M = 0$. The Dirac matrices ($\gamma^0, \gamma^1, \gamma^2, \gamma^3, \gamma^5$) in contravariant notations are $\gamma^0 = \sigma^z \otimes I^{2 \times 2}$, $\gamma^j = i\sigma^y \otimes \tau^j, j = 1, 2, 3$, and $\gamma^5 = i\gamma^0 \gamma^1 \gamma^2 \gamma^3$. The eigenvalues ϵ_j of the Hamiltonian matrix (12) are given by the quartic

$$\epsilon_j^4 + a \epsilon_j^3 + b \epsilon_j^2 + c \epsilon_j + d = 0. \quad (13)$$

The coefficients (a, b, c, d) are given in Appendix A (see Eq. (A.2) -- (A.6)). In view of the Ferrari's solution of a quartic equation, we find the roots as

$$\epsilon_j(s, \sigma, k, b, M) = \epsilon_{j,k}^{s,\sigma}(b) = \sigma \sqrt{\frac{\eta_0(k)}{2}} - \frac{a}{4} + s \left(b_0(k) - \left(\frac{\eta_0(k)}{2} \right) + \sigma c_0(k) \sqrt{\frac{2}{\eta_0(k)}} \right)^{\frac{1}{2}}, \quad (14)$$

where $j=1,2,3,4$, $\sigma = \pm 1$ is the spin index and $s = \pm 1$ is the band-index. Here $\epsilon_{j,k}^{s,\sigma}(b)$ is simply a short-hand notation. The spin-down ($\sigma = -1$) conduction band ($s = +1$) and the spin-up ($\sigma = +1$) valence band ($s = -1$), denoted respectively by $\epsilon_1(s = +1, \sigma = -1, k, b)$ and $\epsilon_2(s = -1, \sigma = +1, k, b)$, are of primary interest as will be shown below. The functions appearing in Eq. (14) are given in Appendix A (see Eq.(A.7)). The eigenstates linked to the eigenvalues in $\epsilon_j(s, \sigma, k, q, \mu, b)$ in (14) are also presented in Appendix A.

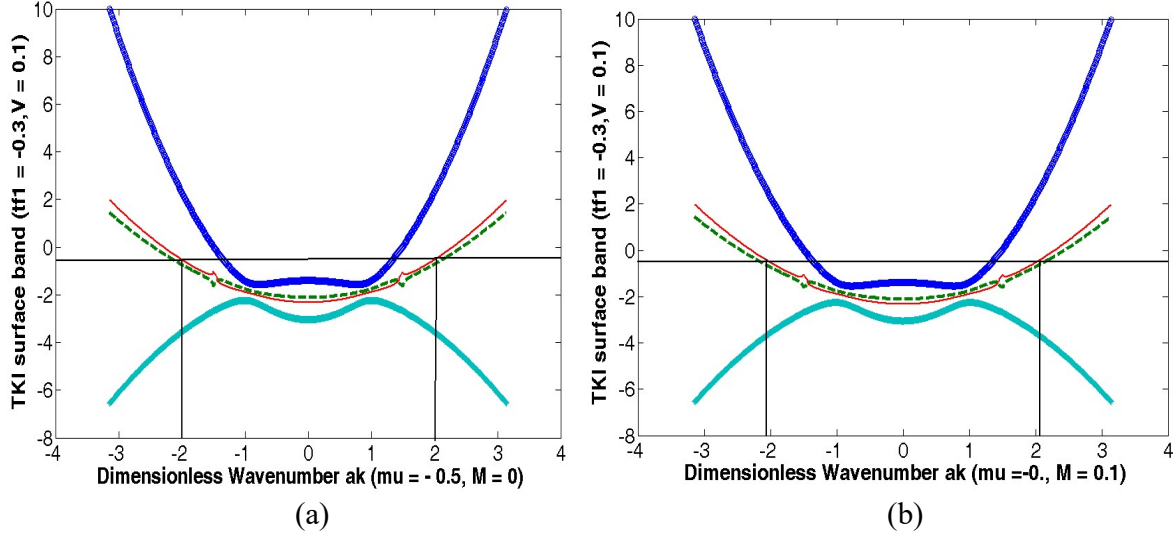


Figure 2. The plots of surface state energy spectrum given by Equation (14) as a function of the dimensionless wave vector ak . The numerical values of the parameters used in the plots are $t_{d_1} = 1$, $t_{f_1} = -0.3$, $t_{d_2} = 0.01$, $t_{f_{n_2}} = 0.01$, $t_{d_3} = 0.001$, $t_{f_3} = 0.001$, $\epsilon_f = -0.02$, $V = 0.1$, $b = 0.98$, $\mu = -0.5$, $M = (0, 0.1)$ and $U_f \gg t_{d_1}$. The horizontal solid line represents the Fermi energy. Since the conduction bands are partially empty, the surface state will be metallic in all the cases. In (a), the system is TR symmetric. Thus, the energy bands of the system come in pairs (i.e. $+k$ state and $-k$ state are at the same energy where $k = 2$), and they are called Kramers pairs. In Figure (b), TR symmetry is lacking and therefore no Kramers pair is possible.

We have plotted the surface state energy spectra given by Eq. (14) as function of the dimensionless wave vector ak in Figures 2(a) and 2(b). Since the conduction bands are partially empty, the surface state will be metallic. In both the figures, t_{f_1} is negative and, therefore, the figures correspond to the insulating bulk. The numerical values of the parameters used in the plots are $t_{d_1} = 1$, $t_{f_1} = -0.3$, $t_{d_2} = 0.01$, $t_{f_2} = 0.01$, $t_{d_3} = 0.001$, $t_{f_3} = 0.001$, $\epsilon_f = -0.02$, $V = 0.1$, $b = 0.98$, $\mu = -0.5$, $\alpha_0 = 0$, $M = 0, 0.3$ and $U_f \gg t_{d_1}$. Here, the red curve (solid line) which corresponds to spin-up valence band ϵ_3 ($s = -1, \sigma = +1, k, b$), and the green curve (dashed line) which corresponds to spin-down conduction band ϵ_2 ($s = +1, \sigma = -1, k, b$), displaying the band-inversion in these figures, are closer to the Fermi energy represented by the horizontal solid line. In Figure 2(a), since $M = 0$, the time reversal symmetry (TRS) is unbroken which is expected to correspond to the quantum spin Hall (QSH) phase. In Figure 2(b), however $M \neq 0$, the time reversal symmetry (TRS) is broken which is expected to correspond to the quantum anomalous Hall (QAH) phase. To support this the calculation of the Chern number (C) is needed. As a quick side note we observe that the states corresponding to momenta $ak = (\pm 2, 0)$ or $(0, \pm 2)$ in Figure 2(a) are degenerate. Furthermore, they satisfy the condition $ak + aG = -ak$ where aG is a reciprocal lattice vector. For example, for $ak = (\pm 2, 0)$ and $aG = (\mp 4, 0)$. Of course, there are other possibilities too, for example $ak = (\pm\sqrt{2}, \pm\sqrt{2})$. These possibilities we are not taking into account for the simple reason that they do not satisfy the condition $k + G =$

$-\mathbf{k}$. Let us now note that the Fermi energy inside the gap intersects the surface state bands in the same BZ, in general, either an even or an odd pair number of times. If there are odd numbers of pair intersections, which guarantees the time reversal invariance, the surface state is topologically non-trivial (strong topological insulator), for moderate disorder (*disorder potential* $\ll t_{d_1}$) cannot remove pairs of such pair-surface-state crossings (SSC). Furthermore, it is also evident that the number of TRIM involved in SSC is one (odd). However, when there are an even number of pair-surface-state crossings, the surface states are topologically trivial (weak TI or ordinary Bloch insulators that are topologically equivalent to the filled shell atomic insulator). The quantized topological numbers, the Kane–Mele index Z_2 for the quantum spin Hall(QSH) phase and the Chern number C for the quantum anomalous Hall (QAH) phase, strongly support such topological states. The QSH band structures are characterized by the topological invariant $\nu_0 = 0$ ($Z_2 = +1$) and $\nu_0 = 1$ ($Z_2 = -1$). The former corresponds to weak TI, while the latter to strong TI. In fact, materials with band structures with $Z_2 = -1$ are expected to exist in systems with strong spin-orbit coupling acting as an internal quantizing magnetic field on the electron system. The graphical representations in Figure 2(a) lead to the indication that the system considered here is a strong TI for $M = 0$. If the indication is corroborated by analysis given below, the TKI surface comprises of ‘helical liquids’, which (helicity) is one of the most unique properties of a topologically protected surface.

In a bid to examine the possibility of helical spin liquids (equivalently, to calculate the Z_2 invariant using the eigenvalues of the space inversion operator), we note that the f - and d -states have different parities, the inversion symmetry (IS) operator in this band basis is constructed as $\Pi = I^{2 \times 2} \otimes \tau^z$. The time reversal (TR) operator for a spin 1/2 particle is $\Theta = I^{2 \times 2} \otimes \tau^y K$. The operator K stands for the complex conjugation. The τ^j are Pauli matrices on two-dimensional spin space. The Hamiltonian under consideration, for $M = 0$, preserves the time reversal (TRS) and inversion symmetries (IS). It can be easily shown that $\langle \Theta \psi | \Theta \phi \rangle = \langle \phi | \psi \rangle$ taking eigenstate of the z -component of the spin operator $I^{2 \times 2} \otimes \tau^z$ as the basis. Also, $\Theta \gamma^0 \Theta^{-1} = \gamma^0$, $\Theta \gamma^5 \Theta^{-1} = \gamma^5$, and $\Theta \gamma^j \Theta^{-1} = -\gamma^j$, where $j = 1, 2$, and 3 . Similarly, $\Pi \gamma^0 \Pi^{-1} = \gamma^0$, $\Pi \gamma^j \Pi^{-1} = -\gamma^j$ ($j = 1, 2$), and $\Pi \gamma^k \Pi^{-1} = \gamma^k$ ($k = 3, 5$). Since only γ^0 and γ^5 are even under time reversal and inversion (and $d_5 = 0$), at a time reversal invariant momentum (TRIM) K_i where the system preserves both TR and IS, the Hamiltonian will have the form $h_{\text{surface}}^{\text{BHZ}}(k = K_i, q, \mu, b, M = 0) = \frac{\epsilon_d + \epsilon_c}{2} I^{4 \times 4} + d_0(k = K_i, q, \mu, b) \gamma^0$. The eigenvalues of γ^0 are ± 1 (multiplicity 2). The corresponding eigenvectors are $|+\rangle = (1/\sqrt{2})(1 \ 1 \ 0 \ 0)^T$ and $|-\rangle = (1/\sqrt{2})(0 \ 0 \ 1 \ 1)^T$. Here $\langle + | \gamma^0 | + \rangle = 1$ and $\langle - | \gamma^0 | - \rangle = -1$. We obtain

$$\begin{aligned} \langle + | h_{\text{surface}}^{\text{BHZ}}(k = K_i, q, \mu, b, M = 0, W_0) | + \rangle &= \epsilon_d = E_+, \\ \langle - | h_{\text{surface}}^{\text{BHZ}}(k = K_i, q, \mu, b, M = 0, W_0) | - \rangle &= \epsilon_c = E_-. \end{aligned} \quad (15)$$

Here

$$d_0 = \frac{\epsilon_d - \epsilon_c}{2}, \epsilon_d = (\epsilon(k, q, \mu, b) + \vartheta(k, q, b)), \epsilon_c = (\epsilon(k, q, \mu, b) - \vartheta(k, q, b)). \quad (16)$$

Obviously enough, if $E_- < E_+$, the state $|-\rangle$ is occupied and the parity of the state at TRIM K_i is -1 . In the opposite case ($E_- > E_+$), the state $|+\rangle$ is occupied and the parity is $+1$. Therefore, the parity is given by $(-sgn[d_0])$.

At this point we make a digression to obtain the result that the Z_2 invariant can be calculated simply by the parity eigenvalues at TRIMs.. The surface states correspond to the eigenstates (or the Bloch states $|\psi^{(\alpha)}(\mathbf{k})\rangle$) linked to the eigenvalues in ϵ_j ($s, \sigma, k, b, M = 0$). These are presented in Appendix A. We consider now a matrix representation of the time reversal (TR) operator Θ in the Bloch wave function basis. With α and β as the band indices we consider the representation is $\xi_{\alpha\beta}(\mathbf{k}) = \langle \psi^{(\alpha)}(-\mathbf{k}) | \Theta | \psi^{(\beta)}(\mathbf{k}) \rangle$. This matrix relates the two Bloch states $|\psi^{(\alpha)}(-\mathbf{k})\rangle$ and $|\psi^{(\beta)}(\mathbf{k})\rangle$ via $|\psi^{(\alpha)}(-\mathbf{k})\rangle = \sum_{\beta} \xi_{\alpha\beta}^*(\mathbf{k}) \Theta |\psi^{(\beta)}(\mathbf{k})\rangle$. With the aid of this one can easily show that $\xi_{\alpha\beta}(\mathbf{k})$ is a unitary matrix ($\xi^\dagger \xi = I$). We also find that it has the property $\xi_{\alpha\beta}(-\mathbf{k}) = -\xi_{\beta\alpha}(\mathbf{k})$. This implies that the matrix $\xi_{\alpha\beta}(K_i)$ at a TRIM becomes anti-symmetric, i.e. $\xi_{\alpha\beta}(K_i) = -\xi_{\beta\alpha}(K_i) \neq 0$. Only when the bands α and β form a Kramers pair, such a non-zero $\xi_{\alpha\beta}$ is obtained. Yet another which we need to consider is the Berry connection matrix defined as $\gamma_{\alpha\beta}(\mathbf{k}) = -i \langle \psi^{(\alpha)}(\mathbf{k}) | \nabla_{\mathbf{k}} | \psi^{(\beta)}(\mathbf{k}) \rangle$. In view of the results $\langle \Theta \psi | \Theta \varphi \rangle = \langle \varphi | \psi \rangle$ and $|\psi^{(\alpha)}(-\mathbf{k})\rangle = \sum_{\beta} \xi_{\alpha\beta}^*(\mathbf{k}) \Theta |\psi^{(\beta)}(\mathbf{k})\rangle$ we arrive at the relation linking $\gamma_{\alpha\beta}(\mathbf{k})$ and $\gamma_{\alpha\beta}(-\mathbf{k})$:

$$\boldsymbol{\gamma}(-\mathbf{k}) = \boldsymbol{\xi}(\mathbf{k}) \boldsymbol{\gamma}^*(\mathbf{k}) \boldsymbol{\xi}^\dagger(\mathbf{k}) + i \boldsymbol{\xi}(\mathbf{k}) \nabla_{\mathbf{k}} \boldsymbol{\xi}^\dagger(\mathbf{k}). \quad (17)$$

Upon taking the trace we find $tr(\boldsymbol{\gamma}(-\mathbf{k})) = tr(\boldsymbol{\gamma}^*(\mathbf{k})) + i tr(\boldsymbol{\xi}(\mathbf{k}) \nabla_{\mathbf{k}} \boldsymbol{\xi}^\dagger(\mathbf{k}))$. Since $\gamma_{\beta\alpha} = \gamma_{\alpha\beta}^*$ and $\xi \nabla \xi^\dagger = -(\nabla \xi) \xi^\dagger$, upon replacing $-\mathbf{k}$ by \mathbf{k} in the preceding equation one may write $\mathbf{A} = tr(\boldsymbol{\gamma}(\mathbf{k})) = tr(\boldsymbol{\gamma}(-\mathbf{k})) + i tr(\boldsymbol{\xi}^\dagger(\mathbf{k}) \nabla_{\mathbf{k}} \boldsymbol{\xi}(\mathbf{k}))$. We shall need this result below. The Berry curvature of $tr(\boldsymbol{\gamma}(\mathbf{k}))$ may be defined as $\boldsymbol{\Omega} = \text{curl} \mathbf{A}$. Since the system preserves the time reversal (TRS) and inversion symmetries (IS), one may select any gauge which renders \mathbf{A} equal to zero. We now consider the anti-symmetric and unitary matrix $\zeta_{\alpha\beta}(\mathbf{k}) = \langle \psi^{(\alpha)}(\mathbf{k}) | \Pi \Theta | \psi^{(\beta)}(\mathbf{k}) \rangle$ (where $\Pi^2 = 1$) to examine the consequence of setting \mathbf{A} equal to zero. Since we find from ref.[13] that $\mathbf{A} = tr(\boldsymbol{\gamma}(\mathbf{k})) = \frac{i}{2} tr(\zeta^\dagger \nabla_{\mathbf{k}} \zeta) = \frac{i}{2} \nabla_{\mathbf{k}} tr(\log \zeta) = i \nabla_{\mathbf{k}} \log(\sqrt{\det[\zeta]})$, it is clear that in order to make $\mathbf{A} = 0$, one needs to adjust the phase of Bloch states $|\psi^{(\alpha)}(\mathbf{k})\rangle$ such that $\text{Pf}(\zeta) = 1$. Suppose now $\rho(K_i^{\text{trim}}) = \pm 1$ are the eigenvalues of Π for band α at TRIM K_i^{trim} , one obtains the matrix

$$\xi_{\alpha\beta}(K_i^{\text{trim}}) = \langle \psi^{(\alpha)}(-K_i^{\text{trim}}) | \Pi \Theta | \psi^{(\beta)}(K_i^{\text{trim}}) \rangle = \zeta_{\alpha\beta}(K_i^{\text{trim}}) \rho_{\alpha}(K_i^{\text{trim}}). \quad (18)$$

Obviously enough, when $\rho_{\alpha} = \rho_{\beta}$, $\xi_{\alpha\beta}(K_i) = -\xi_{\beta\alpha}(K_i) \neq 0$. Only when the bands α and β form a Kramers pair, such a non-zero $\xi_{\alpha\beta}$ is obtained. It follows that if the bands α and β are the n th Kramers pair in the total of $2N$ bands, we may write $\rho_{\alpha} = \rho_{\beta} \equiv \rho_{2n}$. From Eq.(17), one can now see that $\text{Pf}[\xi_{\alpha\beta}(K_i^{\text{trim}})] = \text{Pf}[\zeta_{\alpha\beta}(K_i^{\text{trim}})] \prod_{n=1}^N \rho_{2n}(K_i^{\text{trim}})$. Since $\text{Pf}(\zeta) = 1$, in view of

this result and Eq.(A.16), we find that that the Z_2 invariant can be calculated simply by the parity eigenvalues ρ_{2n} at TRIMs K_i^{trim} , that is $(-1)^{\nu} = \prod_i \delta(K_{\text{trim}}^{(i)}) = \prod_i \prod_n \rho_{2n}(K_{\text{trim}}^{(i)})$.

Upon getting back to Eq.(16) and taking into account the observations below this equation, the parity of the occupied state at $K_{\text{trim}}^{(i)}$, viz. $\delta(K_{\text{trim}}^{(i)})$, is given by $\delta(K_{\text{trim}}^{(i)}) = (-sgn[d_0])$. Besides, from Eq. (A.1), it is easy to infer $\epsilon_c > \epsilon_d$ at a given momentum. This implies that $E_- > E_+$. Regarding the topology of our band system, this in turn leads to the conclusion that $\nu = 1$. This means that the system is a strong topological (non-trivial) insulator.

4.Floquet Theory

The original time-dependent problem (with periodicity in external driving force) could be mapped into effective time-independent formulation in Floquet theory [36]. The theory was used extensively in the past in the theoretical studies of external driving on transport in various systems commissioning combination of the theory with Schrodinger equation [37], Green's functions [38-40], quantum master equation [41,42], scattering matrix approach [43], and so on. The combinations of the Floquet theory with dynamical mean field theory [44], and slave boson protocol [45] were also formulated for strongly correlated systems. Our approach is in acquiescence to the latter. We assume the normal incidence of CPOF on the surface SmB_6 with the thickness $d = 30 \text{ nm}$. Suppose the angular frequency of the optical field incident on the film is $\omega \approx 10^{15} \text{ radian} - s^{-1}$ and wavelength $\lambda_{in} \approx 1500 \text{ nm}$. Therefore the ratio $d/\lambda_{in} \approx 0.02 \ll 1$. Upon taking the field into consideration our Hamiltonian becomes time dependent. The Floquet theory can be applied to our time-periodic Hamiltonian $H_{\text{surface}}(t) = H_{\text{surface}}(t + T)$ with the period $T = 2\pi/\omega$. Analogous to the Bloch theory involving quasi-momentum, a solution $|\eta(t)\rangle = \exp(-i\dot{\epsilon}t) |\xi(t)\rangle$ involving the Floquet quasi-energy $\dot{\epsilon}$ could be written down for the time-dependent Schrodinger equation of the system. The Floquet state satisfies $|\xi(t)\rangle = |\xi(t + T)\rangle$ and, therefore, could be expanded in a Fourier series $|\xi(t)\rangle = \sum_r \exp(-ir\omega t) |\xi_r\rangle$ where r is an integer. Then the wave function, in terms of the quasi-energy $\dot{\epsilon}$ has the form $|\eta(t)\rangle = \sum_r \exp\left(-i\left(\frac{\dot{\epsilon}}{\hbar} + r\omega\right)t\right) |\xi_r\rangle$. This makes us arrive at an infinite dimensional eigenvalue equation in the Sambe space (the extended Hilbert space)[26]:

$$\sum_s H_{\text{surface},r,s} |\xi_n^s\rangle = (s\hbar\omega\delta_{r,s} + \frac{1}{T} \int_0^T H_{\text{surface}}(t) e^{i(r-s)\omega t} dt) |\xi_n^s\rangle = \dot{\epsilon}_n |\xi_n^s\rangle. \quad (19)$$

The matrix element $H_{\text{surface},\alpha,\beta}$ is given by $H_{\text{surface},\alpha,\beta} = \alpha\hbar\omega\delta_{\alpha,\beta} + \frac{1}{T} \int_0^T H_{\text{surface}}(t) e^{i(\alpha-\beta)\omega t} dt$, where (α, β) are integers. This is the Floquet state surface Hamiltonian of the system. One can now write

$$H_{\text{surface},\alpha,\beta} = \begin{pmatrix} \cdots & \cdots & \cdots & \cdots & \cdots \\ \cdots & H_{\text{surface},-1,-1} & H_{\text{surface},-1,0} & H_{\text{surface},-1,1} & \cdots \\ \cdots & H_{\text{surface},0,-1} & H_{\text{surface},0,0} & H_{\text{surface},0,1} & \cdots \\ \cdots & H_{\text{surface},1,-1} & H_{\text{surface},1,0} & H_{\text{surface},1,1} & \cdots \\ \cdots & \cdots & \cdots & \cdots & \cdots \end{pmatrix}. \quad (20)$$

The optical field $\mathbf{E}(t)$ may be expressed in terms of the electric scalar potential (assumed to be zero) and the time-varying magnetic vector potential $\mathbf{A}(t) = \mathbf{A}(t + T) = \mathbf{A}_1(\sin(\omega t), \sin(\omega t + \psi), 0)$ through the relation: $\mathbf{E}(t) = -\frac{\partial \mathbf{A}(t)}{\partial t} = -\mathbf{E}(\cos(\omega t), \cos(\omega t + \psi), 0)$, $\mathbf{E} = \mathbf{A}_1 \omega$. In particular, when the phase $\psi = 0$ or π , the optical field is linearly polarized. When $\psi = +\pi/2$ ($\psi = -\pi/2$), the optical field is left-handed (right-handed) circularly polarized. Once we have included a gauge field, it is necessary that we make the Peierls substitution $H_{surface}(t, b) = H_{surface}\left(\mathbf{k} - \frac{e}{\hbar} \mathbf{A}(t), b\right)$. The quantity $aA_0 = \frac{aeE}{\hbar\omega}$ corresponds to the light intensity. It is a dimensionless quantity. In view of the Floquet theory [24-29], we can now write a static effective Hamiltonian, in the off-resonant regime using the Floquet-Magnus (high-frequency) expansion [27]:

$$H_{surface}^{Floquet}(k) = H_{surface,0,0} + \frac{[H_{surface,0,-1}, H_{surface,0,1}]}{\hbar\omega} + O(\omega^{-2}), \quad (21)$$

where $H_{surface,n,m} = \frac{1}{T} \int_0^T H_{surface}(t) e^{i(n-m)\omega t} dt$ with $n \neq m$. For $M = 0$, as we have seen in the previous section, we obtain QSH state with the net Hall conductance of the system described by Eq.(10) as zero. We now consider the same QSH insulator and write

$$H_{surface,0,0} = h_{surface}(k, q, \mu, b) + \left[\frac{t_{d1} + b^2 t_{f1}}{2} + 2(t_{d2} + b^2 t_{f2}) + 2(t_{d3} + b^2 t_{f3}) \right] \\ \times (a^2 A_0^2) \sigma_0 \otimes \tau_0 + \left[\frac{t_{d1} - b^2 t_{f1}}{2} + 2(t_{d2} - b^2 t_{f2}) + 2(t_{d3} - b^2 t_{f3}) \right] (a^2 A_0^2) \sigma_0 \otimes \tau_z, \quad (22)$$

$$H_{surface,0,-1} = - \left[\frac{t_{d1} + b^2 t_{f1}}{2} + 2(t_{d2} + b^2 t_{f2}) + 2(t_{d3} + b^2 t_{f3}) \right] ia^2 (k_x + e^{-i\psi} k_y) A_0 \sigma_0 \otimes \tau_0 \\ - \left[\frac{t_{d1} - b^2 t_{f1}}{2} + 2(t_{d2} - b^2 t_{f2}) + 2(t_{d3} - b^2 t_{f3}) \right] ia^2 (k_x + e^{-i\psi} k_y) A_0 \sigma_0 \otimes \tau_z \\ - (i/2) A_1 (aA_0) \sigma_z \otimes \tau_x - (i/2) A_1 (aA_0) e^{-i\psi} \sigma_0 \otimes \tau_y, \quad (23)$$

$$H_{surface,0,1} = \left[\frac{t_{d1} + b^2 t_{f1}}{2} + 2(t_{d2} + b^2 t_{f2}) + 2(t_{d3} + b^2 t_{f3}) \right] ia^2 (k_x + e^{i\psi} k_y) A_0 \sigma_0 \otimes \tau_0 \\ + \left[\frac{t_{d1} - b^2 t_{f1}}{2} + 2(t_{d2} - b^2 t_{f2}) + 2(t_{d3} - b^2 t_{f3}) \right] ia^2 (k_x + e^{i\psi} k_y) A_0 \sigma_0 \otimes \tau_z \\ + (i/2) A_1 (aA_0) \sigma_z \otimes \tau_x + (i/2) A_1 (aA_0) e^{i\psi} \sigma_0 \otimes \tau_y. \quad (24)$$

From the action of the time reversal operator on the wave function we see, that it leads to a complex conjugation of the wave function. Thus, in the case of spin-less wave functions as $\Theta = K$, where K is the operator for complex conjugation. More generally, we can write $\Theta = UK$ where U is a unitary operator. Furthermore, for a spin-1/2 particle, flipping the spin coincides with the time-reversal.

This means $\Theta \widehat{\mathcal{S}} = -\widehat{\mathcal{S}}$ where $\widehat{\mathcal{S}} = \frac{1}{2} \widehat{\sigma}$ and $\widehat{\sigma}$ is the vector of Pauli matrices. In view of these, one may also choose $\Theta = i\sigma_y \otimes \tau_0 K$. Upon making use of the results $\Theta \widehat{A} \Theta^{-1} = \widehat{A}$, $\Theta \widehat{B} \Theta^{-1} = -\widehat{B}$, and so on, where $\widehat{A} = \sigma_0 \otimes \tau_0$, $\sigma_z \otimes \tau_y$, ... and $\widehat{B} = \sigma_0 \otimes \tau_y$,, we find that

$$\begin{aligned} & \Theta H_{\text{surface}}^{\text{Floquet}}(ak_x, ak_y) \Theta^{-1} \\ &= H_{\text{surface}}^{\text{Floquet}}(-ak_x, -ak_y) + (4a^2 A_0^2 \sin\psi / \hbar\omega) \{A_1 ak_x \sigma_0 \otimes \tau_x + A_1 ak_y \sigma_z \otimes \tau_y\} \\ &\times \left[\frac{t_{d1} + b^2 t_{f1}}{2} + 2(t_{d2} + b^2 t_{f2}) + 2(t_{d3} + b^2 t_{f3}) \right] + \left(\frac{4a^2 A_0^2 A_1^2 \sin\psi}{\hbar\omega} \right) \sigma_z \otimes \tau_z, \end{aligned} \quad (25)$$

where $\Theta H_{\text{surface}}^{\text{Floquet}}(ak_x, ak_y) \Theta^{-1} = H_{\text{surface}}^{\text{Floquet}}(k)(-ak_x, -ak_y)$ only when $\psi = 0$ or π , that is, when the optical field is linearly polarized. In this case, the time reversal symmetry (TRS) is not broken. However, when $\psi \neq 0$ or π , TRS is broken. We now consider the particular cases where $\psi = +\pi/2$ and $\psi = -\pi/2$. For the former the optical field is left-handed circularly polarized, whereas for the latter it is right-handed. Thus, the (previously not known) consequence is that the incidence of the CPOF on the Bi2212 surface will be able to create a QSH insulator with the broken TRS.

The Hamiltonian to describe this broken TRS system, in the basis $(d_{k,\uparrow}^\dagger \ bc_{k,\downarrow}^\dagger \ d_{k,\downarrow}^\dagger \ bc_{k,\uparrow}^\dagger)^\top$, could be written as $H_{\text{surface}}^{\text{Floquet}}(k) =$

$$\begin{pmatrix} E_1 & A_{10P}^+(ak_-) & 0 & -i A_{10P}^+ aq \\ A_{10P}^+(ak_+) & E_2 & -i A_{10P}^+ aq & 0 \\ 0 & i A_{10P}^- aq & E_3 & -A_{10P}^-(ak_-) \\ i A_{10P}^- aq & 0 & -A_{10P}^-(ak_+) & E_4 \end{pmatrix} \quad (26)$$

where $ak_{\mp} = ak_x \mp iak_y$, $E_1 = \epsilon_{OP} + \vartheta_{OP}^+$, $E_2 = \epsilon_{OP} - \vartheta_{OP}^+$, $E_3 = \epsilon_{OP} + \vartheta_{OP}^-$, $E_4 = \epsilon_{OP} - \vartheta_{OP}^-$, $A_{10P}^\pm = A_1 \left(1 \pm 2B_2 \sin\psi \left(\frac{a^2 A_0^2}{\hbar\omega} \right) \right)$, and $A_1 = 2Vb$. The eigenvalues (ϵ_α) of the matrix (26) is given by the quartic $\epsilon_\alpha^4 + \gamma_{10}(k, b) \epsilon_\alpha^3 + \gamma_{20P}(k, b) \epsilon_\alpha^2 + \gamma_{30P}(k, b) \epsilon_\alpha + \gamma_{40P}(k, b) = 0$ ($\alpha = 1, 2, 3, 4$) where the coefficients $\gamma_{\beta 0P}(k, b)$ ($\beta = 1, 2, 3, 4$) are given by

$$\gamma_{10P}(k, b) = -\sum_{\mu} E_{\mu}, \gamma_{20P}(k, b) = \left(\frac{1}{2}\right) \sum_{\mu \neq \nu} E_{\mu} E_{\nu} - 2(A_{10P}^+ A_{10P}^-)(aq)^2 - (A_{10P}^+)^2 + A_{10P}^-^2)(ak)^2, \quad (27)$$

$$\gamma_{30P}(k, b) = \left(-\frac{1}{6}\right) \sum_{\mu \neq \nu \neq \sigma} E_{\mu} E_{\nu} E_{\sigma} + (A_{10P}^+ A_{10P}^-)(aq)^2 \sum_{\mu} E_{\mu} + A_{10P}^-^2 (ak)^2 (E_1 + E_2) +$$

$$A_{10P}^{+2}(ak)^2(E_3 + E_4), \quad (28)$$

$$\begin{aligned} \gamma_{40P}(k) = & \prod_{\mu} E_{\mu} - A_{10P}^{-2}(ak)^2(E_1E_2) - A_{10P}^{+2}(ak)^2(E_3E_4) - A_{10P}^{+}A_{10P}^{-}(aq)^2(E_1E_4 + E_2E_3) + \\ & A_{10P}^{-2}A_{10P}^{+2}(ak)^4 + A_{10P}^{-2}A_{10P}^{+2}(aq)^4 - 2A_{10P}^{-2}A_{10P}^{+2}(aq)^2((ak_x)^2 - (ak_y)^2). \end{aligned} \quad (29)$$

It may be noted that to denote these eigenvalues we have used the symbol *var epsilon* which is distinct from that in Eq. (13). The functions ϵ_{OP} and ϑ_{OP}^{\pm} are given by

$$\begin{aligned} \epsilon_{OP}(k, q, \mu, b) = & \epsilon_0(\mu, b) - D_1(b)a^2q^2 + D_2(b)a^2k^2 + a^2A_0^2D_2(b) + O(a^4k^4), \\ \vartheta_{OP}^{\pm}(k, q, b) = & \vartheta_0(b) - B_1(b)a^2q^2 + B_2(b)a^2k^2 - \left(a^2A_0^2B_2 \pm \left(\frac{a^2A_0^2}{\hbar\omega} \right) \sin\psi A_1^2 \right). \end{aligned} \quad (30)$$

Once again, in view of the Ferrari's solution of a quartic equation, we find the roots as

$$\begin{aligned} \epsilon_{\alpha}(s, \sigma, k, b) = & \mu \sqrt{\frac{\eta_{OP}(k)}{2} - \frac{\gamma_{10P}(k,b)}{4}} + l \left(b_{OP}(k) - \left(\frac{\eta_{OP}(k)}{2} \right) + \right. \\ & \left. \mu c_{OP}(k) \sqrt{\frac{2}{\eta_{OP}(k)}} \right)^{\frac{1}{2}}. \end{aligned} \quad (31)$$

where $\alpha = 1, 2, 3, 4$, $\mu = \pm 1$ is the spin index and $l = \pm 1$ is the band-index. The spin-down ($\mu = -1$) conduction band ($l = +1$) and the spin-up ($\mu = +1$) valence band ($l = -1$), denoted respectively by $\epsilon_2(l = +1, \mu = -1, k, b)$ and $\epsilon_3(l = -1, \mu = +1, k, b)$, are somewhat peculiar as will be shown below. The functions appearing in Eq. (31) are given by

$$\begin{aligned} \eta_{OP}(k) = & \frac{2b_{OP}(k)}{3} + (\Delta_{OP}(k) - \Delta_{00P}(k))^{\frac{1}{3}} - (\Delta_{OP}(k) + \Delta_{00P}(k))^{\frac{1}{3}}, \\ \Delta_{00P}(k) = & \left(\frac{b_{OP}^3(k)}{27} - \frac{b_{OP}(k)d_{OP}(k)}{3} - c_{OP}^2(k) \right), \\ \Delta_{OP}(k) = & \left(\frac{2}{729}b_{OP}^6 + \frac{4d_{OP}^2b_{OP}^2}{27} + c_{OP}^4 - \frac{d_{OP}b_{OP}^4}{81} - \frac{2b_{OP}^3}{27} + \frac{2c_{OP}^2b_{OP}d_{OP}}{3} + \frac{d_{OP}^3}{27} \right)^{1/2}, \\ b_{OP}(k) = & \left\{ \frac{3\gamma_{10P}(k,b)^2 - 8\gamma_{20P}(k,b)}{16} \right\}, \quad c_{OP}(k) = \left\{ \frac{-\gamma_{10P}(k,b)^3 + 4\gamma_{10P}(k,b)\gamma_{20P}(k,b) - 8\gamma_{30P}(k,b)}{32} \right\}, \\ d_{OP}(k) = & \frac{-3\gamma_{10P}(k,b)^4 + 256\gamma_{40P}(k,b) - 64\gamma_{10P}(k,b)\gamma_{30P}(k,b) + 16\gamma_{10P}(k,b)^2\gamma_{20P}(k,b)}{256}. \end{aligned} \quad (32)$$

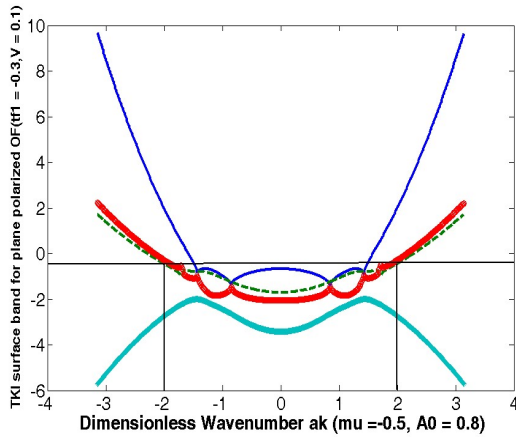
The eigenvectors corresponding to $\epsilon'_{\alpha}s$ could be calculated in a manner given in the Appendix A. The value of $a^2A_0^2$ (dimensionless intensity of the radiation) is taken to be around 0.8 which is

good enough for the radiation field of frequency $\nu \sim 3 \times 10^{14} \text{ Hz}$ under consideration. **Moreover, $\sin\psi = +1$ ($\sin\psi = -1$ sign) corresponds to the left-handed (right-handed) circularly polarized radiation above.** We notice from Eq.(30) that CPOF not only renormalizes d and f electron hopping integrals but also does the renormalization of the hybridization parameter(HP).

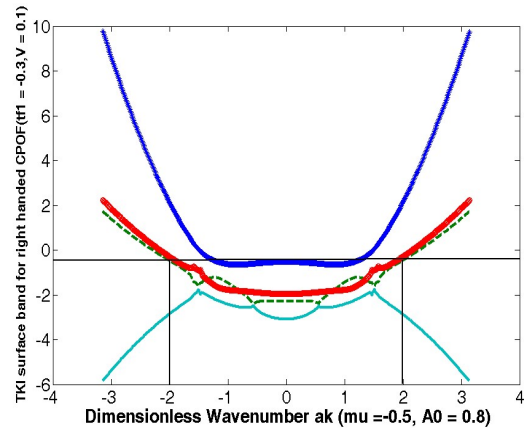
We have the renormalized hybridization parameters(HP) as $A_{1OP}^{\pm} = A_1 \left(1 \pm 2B_2 \sin\psi \left(\frac{a^2 A_0^2}{\hbar\omega} \right) \right)$,

and $A_1 = 2Vb$. As $B_2(b) \approx \left[\frac{t_{d1} - b^2 t_{f1}}{2} \right] > 0$, we find that the renormalized HP $A_{1OP}^+ > A_1$ ($A_{1OP}^+ < A_1$) for the left-handed (right-handed) CPOF. However, the renormalized HP $A_{1OP}^- < A_1$ ($A_{1OP}^- > A_1$) for the left-handed(right-handed) CPOF. We note that, principle, when a renormalized parameter(RHP) is less than A_1 , it is possible that there is a critical intensity of the radiation $a^2 A_0^2 \approx \frac{(\hbar\omega)}{(t_{d1} - b^2 t_{f1})}$ at a given frequency at which the RHP in question will be zero. This, however, may affect the topological nature of the material. Now the nearest neighbor hopping elements t_{d1} and t_{f1} are related to the band masses by $t_{d1, f1} \approx \frac{\hbar^2}{2m_{d,f} a^2}$. If one takes for the band masses $m_d(m_f) = 1.5 m_e$ ($50 m_e$), where m_e is the rest mass of the electron, then the corresponding values of the hopping matrix elements are $t_{d1} \approx 150 \text{ meV}$ and $t_{f1} \approx 4.5 \text{ meV}$. This yields the critical intensity of the radiation $a^2 A_0^2 \approx 2.25$ which is roughly 2.8 times the intensity value assumed in the graphical representations in Figure 3.

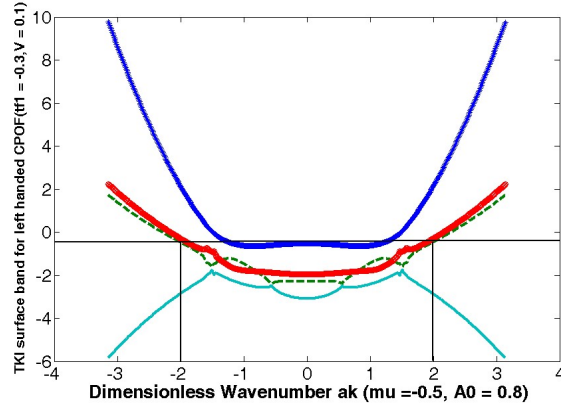
In Figure 3 (a) we have plotted the energy eigenvalues $\varepsilon_{\alpha}(s, \sigma, k, b)$ as a function of ak for a given $aA_0 = 0.80$ for the plane polarized light. In Figures 3(b) and 3(c), respectively, the plots are for the right-handed and the left-handed CPOF; the value of aA_0 remains the same. The numerical values of the parameters used in the plots are $t_{d1} = 1, t_{f1} = -0.3, t_{d2} = 0.01, t_{f_{n2}} = 0.01, t_{d3} = 0.001, t_{f3} = 0.001, \epsilon_f = -0.02, V = 0.1, b = 0.98, \mu = -0.5, M = 0$ and $U_f \gg t_{d1}$. The horizontal solid line represents the Fermi energy. The spin-down conduction band ($l = +1$) and the spin-up valence band ($l = -1$), denoted respectively by $\varepsilon_2(l = +1, \mu = -1, k, b)$ and $\varepsilon_3(l = -1, \mu = +1, k, b)$ represented by solid red lines and dashed green lines respectively, apart from the band-inversion, exhibit some peculiarities by way of the multiple avoided crossings. This



(a)



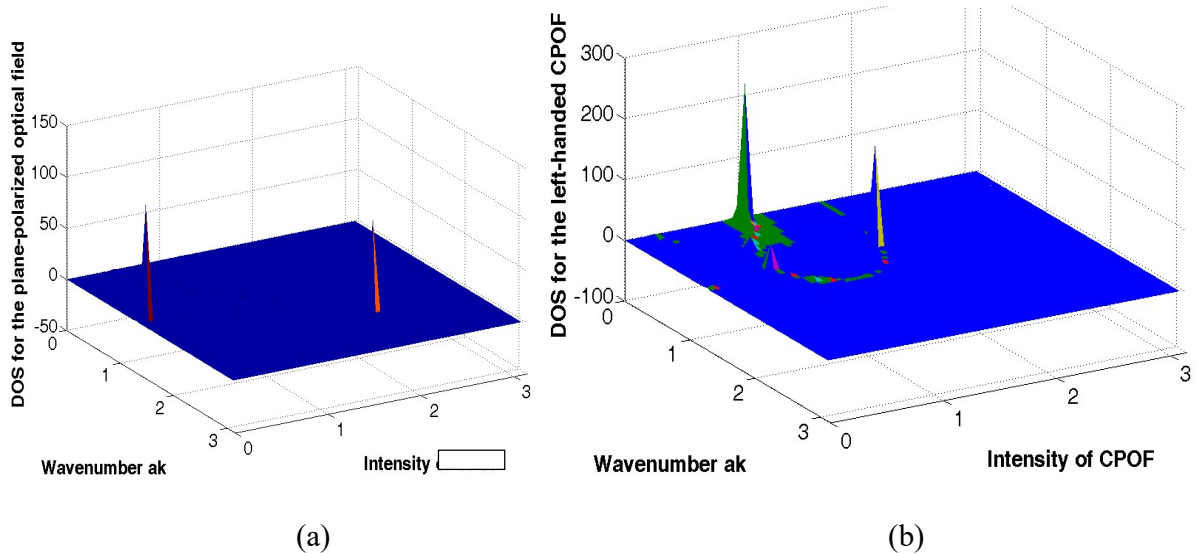
(b)



(c)

Figure 3. The plots of energy eigenvalues $\varepsilon_\alpha(s, \sigma, k, b)$ in Eq.(31) as a function of ak for a given intensity of incident radiation $aA_0 = 0.80$. In Figure (a), the plot is for the plane polarized light. In Figures 3(b) and 3(c), respectively, the plots are for the right-handed and the left-handed CPOF; the value of aA_0 remains the same. The numerical values of the parameters used in the plots are $t_{d_1} = 1$, $t_{f_1} = -0.3$, $t_{d_2} = 0.01$, $t_{f_{n2}} = 0.01$, $t_{d_3} = 0.001$, $t_{f_3} = 0.001$, $\epsilon_f = -0.02$, $V = 0.1$, $b = 0.98$, $\mu = -0.5$, $M = 0$ and $U_f \gg t_{d_1}$. The horizontal solid line represents the Fermi energy.

non-trivial feature is beyond our current understanding at the moment. The figures show that, whether TRS is preserved (as in Figure 3(a)) or it is broken (as in Figures 3(b) and 3(c)), the emergent QSH phase of the system is very robust. The reason being in all the three figures the Fermi energy intersects the band $\varepsilon_3(l = -1, \mu = +1, k, b)$ only in the same BZ an odd pair number of times. This pair of surface state crossings (SSC) corresponds to momenta $\mathbf{k} = (\pm 2, 0)$ or $(0, \pm 2)$. These momenta satisfy the condition $a\mathbf{k} + a\mathbf{G} = -a\mathbf{k}$, where the reciprocal lattice vector



(a)

(b)

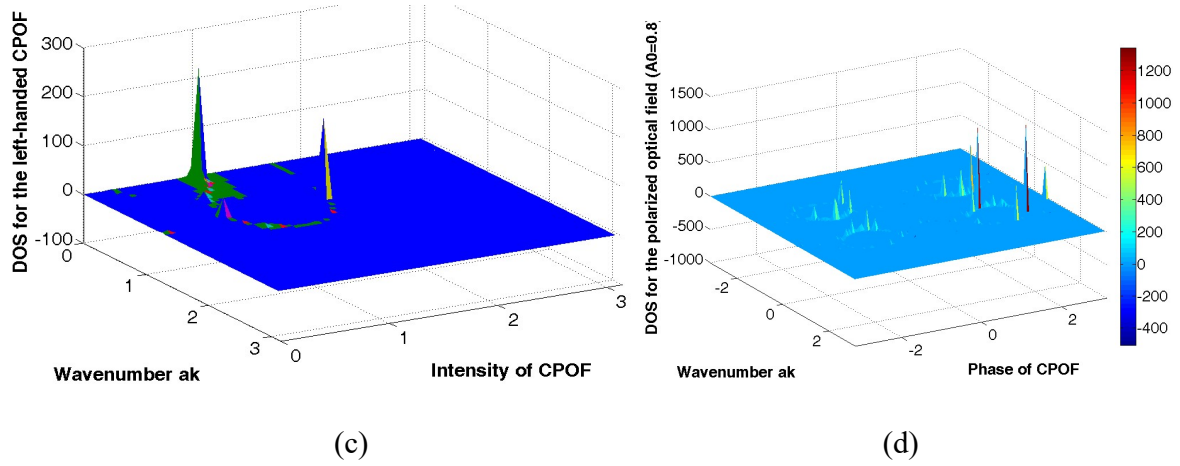


Figure 4. The 3D plots of DOS for the plane-polarized light (Figure 4(a)), the left-handed CPOF (Figure 4(b)), and the right-handed CPOF (Figure 4(c)) as a function of the dimensionless wavevector and the intensity of the incident radiation. In Figure 4(d) we have plotted DOS corresponding to the polarized optical field as a function of the dimensionless wavevector and the phase ψ of the incident radiation. The numerical values of the parameters used in the plots are $t_{d_1} = 1$, $t_{f_1} = -0.175$, $t_{d_2} = 0.01$, $t_{f_{n2}} = 0.01$, $t_{d_3} = 0.001$, $t_{f_3} = 0.001$, $\epsilon_f = -0.02$, $V = 0.1$, $b = 0.98$, $\mu = -0.5$, $M = 0$, $\epsilon = 0.1$. and $U_f \gg t_{d_1}$.

\mathbf{G} is $(\mp 4, 0)$ or $(0, \mp 4)$. We have checked that our graphical representation analysis leads to the fact that the emergent unconventional QSH phase, obtained due to the light-matter interaction, also features robustness to random disorder scattering in the cases of the right-handed as well as the left-handed CPOF.

We now wish to examine how the dimensionless density of states (DOS) changes under the influence of CPOF. The dimensionless DOS $\rho(k, \omega) \equiv \left(-\frac{1}{2\pi^2}\right) \rho_0^{-1} \text{Im } G^R(k, \omega)$ where we take a broad bandwidth, say $(10t_{d_1})$, which gives $\rho_0^{-1} = 10t_{d_1}$ while the single-particle spectral function is given by $\zeta(k, \omega) = (-\pi^{-1}) \text{Im } G^R(k, \omega)$. The retarded Green's function given by: $G^R(k, \omega) = \int_{-\infty}^{+\infty} \frac{d\omega'}{2\pi} \frac{\zeta(k, \omega')}{(\omega - \omega' + i0^+)}$. Upon doing a little analysis we obtain the equation of motion of the Green's functions $G_0(k\sigma, \tau) = -\langle T_\tau \{d_{k\sigma}(\tau) d_{k\sigma}^\dagger(0)\} \rangle$, $F_0(k\sigma, \tau) = -b^2 \langle T_\tau \{c_{k\sigma}(\tau) d_{k\sigma}^\dagger(0)\} \rangle$, etc., where T_τ is the time-ordering operator which arranges other operators from right to left in the ascending order of imaginary time τ . These are the functions to the lowest order without the effect of the impurity scattering incorporated into them. The Fourier coefficients (FCs) of the thermal averages are given by $G_0(k, z) = \int_0^\beta \frac{d\tau}{2\pi} \exp(z\tau) G_0(k, \tau)$ where $z = i\omega_n$, and the Matsubara frequencies are $\omega_n = \left[\frac{(2n+1)\pi}{\beta}\right]$ with $n = 0, \pm 1, \pm 2, \dots$. We obtain the corresponding FC's, for example $\frac{1}{G_0(k, z)} \approx [z - \epsilon_\alpha - \Sigma(k, z)]$. The imaginary part of the self-energy $\Sigma(k, z)$ of the conduction electrons, in the context of electron-phonon interaction, could be modeled as $(-\hbar/\tau)$ (where τ is the relaxation time), say, for $|\epsilon_\alpha - \mu| > \hbar\omega_c$ where ω_c is a characteristic frequency of phonons. For $|\epsilon_\alpha - \mu| < \hbar\omega_c$, the imaginary part will be $-(\epsilon_\alpha - \mu)/\hbar\omega_c)^2 (\hbar/\tau)$. The real part of the $\Sigma(k, z)$ could be obtained by the Kramers-Kronig relations. Upon using Sokhatsky-Plemelj (SP) identity $(x \pm i0^+)^{-1} = [P\left(\frac{1}{x}\right) \mp i\pi\delta(x)]$, where P represents a Cauchy's principal value, one can express $G_0(k, z)$ in a convenient form: $G_0(k, z) =$

$\sum (z - \varepsilon_\alpha - \Sigma)^{-1} A_0^{(\alpha)}$. The spectral function $\zeta_0(k, \omega)$ calculated using $i\zeta_0(k, \omega) = \{G_0(k, z)|_{z=\omega-i0^+} - G_0(k, z)|_{z=\omega+i0^+}\}$. Upon using SP identity once again we find that $\rho(k, \omega)$ without the effect of the impurity scattering is given by a sum of δ functions at the quasi-particle energies. We adopt the definition of the delta function as a limit of a Lorentzian: $\delta(x) \equiv (1/\pi) \lim_{\varepsilon \rightarrow 0} [\varepsilon / (\varepsilon^2 + x^2)]$, and approximate this as a Lorentzian with a small width 2ε in our pictorial representations in Figure 4. In this figure we have 3D plotted DOS for the plane-polarized light (Figure 4(a)), the left-handed CPOF (Figure 4(b)), and the right-handed CPOF (Figure 4(c)). as function of the dimensionless wavevector and the intensity of the incident radiation. In Figure 4(d) we have plotted DOS corresponding to the polarized optical field as function of the dimensionless wavevector and the phase ψ of the incident radiation. The numerical values of the parameters used in the plots are $t_{d_1} = 1$, $t_{f_1} = -0.175$, $t_{d_2} = 0.01$, $t_{f_{n_2}} = 0.01$, $t_{d_3} = 0.001$, $t_{f_3} = 0.001$, $\varepsilon_f = -0.02$, $V = 0.1$, $b = 0.98$, $\mu = -0.5$, $M = 0$, $\varepsilon = 0.1$. and $U_f \gg t_{d_1}$. Upon comparison between Figures 4(a) – 4(c) we notice a growth of DOS in the CPOFs compared to that in the case of the plane-polarized light. The Figure 4(d) corroborates this featuring larger DOS in the CPOF cases.

5. Discussion and concluding remarks

As already stated, the strong correlation effects and diverse surface conditions make the GTKI system extremely complicated and almost a Gordian knot. We summarize these complications to bring home the point that the system needs concerted investigation. In the quantum oscillation experiments of Li et al. [46], within the bulk hybridization gap, the signatures of two-dimensional Fermi surfaces on (100) and (101) surface planes supporting the presence of topological surface states were obtained. Tan et al. [47] and, subsequently, Hartstein et al. [48], uncovered a deep mystery associated with the insulating bulk of SmB₆, which is the formation of a large three-dimensional (solely) conduction electron FS in the absence of the long-range charge transport, given that thus far such FSs have been considered the preserve of metals. Their observation is that the FS is unconventional in an insulating bulk in the absence of a Fermi liquid in SmB₆ system. The oddity was initially conjectured to be due to the residual density of states at the Fermi energy in SmB₆. The existence of the residual DOS was indicated through measurements of heat capacity [49] long ago. Later on, various theoretical models that invoke novel itinerant low-energy neutral excitations (majoranas)[50] within the charge gap that can produce magneto quantum oscillation (MQO) signals have been proposed. The theoretical models which entered the fray are based on magnetoexcitons [51], scalar Majorana fermions [52], emergent fractionalized quasiparticles [53, 54] and non-Hermitian states [55]. In the microscopic approach in ref.[54], in particular, it was shown that a repulsive density–density interaction between the f and d –electrons representing an attractive interaction between the \tilde{f} –hole (obtained using a particle-hole transformation involving a fully antisymmetric tensor) and the d –electron leads to the formation of electrically neutral fermionic quasiparticle conglomerate referred to as the ‘composite exciton Fermi liquid (CEFL)’. The liquid, with electrically neutral bulk, hosts a three dimensional, stable Fermi surface of CEFL induced by an emergent U(1) gauge field. It shares this property with the ground state of the mixed valence compound SmB₆. As has been reported earlier [51], in SmB₆, the QOs are observed only

in the magnetization (de Haas-van Alphen(dHvA)effect). The dHvA oscillations strongly deviate below 1 K from the Lifshitz-Kosevich theory (LKT), which is based on Fermi liquid theory(FLT)[56]. This puts a question mark on any work on SmB₆ leaning on FLT. An example of this kind is the work of LaBarre et al.[57]. The authors include the contribution from phonons as well as the electronic contribution to the total specific heat $C(T)$. Invoking the fact that the large variation in $C(T)$ among different samples [58-61], the authors [57] implicitly contend that it is entirely plausible that the thermal conductivity is also plagued by sample quality uncertainty. We do agree that the rare-earth purification is exceedingly difficult. Coming back to the issue of NFL, as pointed out in ref.[50], the elusive particle majoranas plus conduction electrons lead to topological Kondo effect which in turn to non-Fermi liquid (NFL) Kondo physics (non-integer power law for the conductance). This is similar to the conduction electrons plus quantum spins with degenerate levels lead to Kondo effect. It must be mentioned that the QOs in YbB₁₂ (a close cousin of SmB₆) are observed in both magnetization (the de Haas-van Alphen, dHvA, effect) and resistivity (the Shubnikov-de Haas, SdH, effect) at applied magnetic fields H where the hybridization gap is still finite. The temperature-dependence of the oscillation amplitude complies with the expectations of Fermi-liquid theory [62]. Moreover, in YbB₁₂, a finite residual temperature-linear term in the thermal conductivity $\kappa/T(T \rightarrow 0)$ is observed demonstrating the presence of gapless and itinerant neutral fermions [63]. On the other hand, $\kappa/T(T \rightarrow 0)$ in SmB₆ has been controversial [60,61]. While $\kappa/T(T \rightarrow 0)$ of SmB₆ has been reported to be very small but finite [64,65,69], the absence of $\kappa/T(T \rightarrow 0)$ has been reported in references [65,66]. It is worth mentioning that in ref.[53] $\kappa/T(T \rightarrow 0)$ has been shown to be finite.

The irreproducibility is possibly due to rare-earth impurities or in the density of mid-gap states. It may have its origin in fledgling Kondo insulating scale in SmB₆ which is extremely vulnerable against a moderate degree of disorder [66,67]. It is well-known [68-70] that research into the role of impurities in SmB₆ spans over 40 years. In fact, these impurities form defects in the coherent Kondo lattice. These are so called “Kondo holes.” Theoretical studies propose non-trivial electronic states in the vicinity of the Kondo holes [71]. In fact, doping Gd, La, etc. as Kondo holes into SmB₆ produces an approximately T-independent Sommerfeld coefficient and increased susceptibility [72]. Recently, Fuhrman et al [60] have found a relationship between specific heat and impurity moment screening (in, say, gadolinium-doped samples) which scales systematically. Abele et al. [73] have argued that the in-gap impurity states form for exceptionally small values of the impurity potential comparable to the hybridization gap which may explain why topological Kondo insulators(TKI) are found to be exceptionally sensitive to impurities. There are other contentious issues too. For instance, it has been shown theoretically by Sollie and Schlottmann [74] way back in 1991 that f vacancies in Kondo insulators produce hybridization in-gap bound states. Furthermore, they argued that instead of being localized at respective sites, there is spread equally over the surrounding nearest neighbor shell of atoms. In Raman scattering experiments [75], only a small concentration of about 1% of vacancies is sufficient to close the gap. In another work [76], it was shown that approximately 4% vacancies may close the gap. As measured in transmission mode quite some time ago, Laurita et al. [77] have shown that there is very high

resistance of the bulk optical conductivity in the THz frequency range. The system, however, shows an extremely large ac conductivity indicating the existence of localized in-gap states. But the investigators [77] were unable to determine whether the ac conductivity was due to surface or bulk states. Yet another example to elucidate the complication is as follows: The photon-energy and -polarization dependent Spin-resolved ARPES (SARPES) measurements were carried out by Xu et al.[78] in the not so distant past. A consistent spin-momentum locked spin texture is obtained for various incident photon energies was obtained by these investigators. The measured spin polarizations reflect certain spin structure. Since the non-intrinsic spin signal strongly depends on the energy and polarization of incident photon, and as the spin polarization of the photoelectrons observed by Xu et al. does not depend on photon polarization, we have a possibility from ref.[78] that the above-mentioned spin structure is intrinsic. In contrast, Suga et al.[79] have reported that the non-intrinsic spin signal (this signal depends strongly on the energy and the polarization of the incident photon) of the localized f states in SmB_6 vanishes with linearly polarized optical field and changes direction when the field changes from left to right circularly polarized.

Upon going back to the spin-polarized ARPES measurements which appear to confirm the surface helical spin texture [78], it would be interesting to see how does surface state react to Rashba splitting as there is evidence of for a massive surface state at the surface Brillouin zone center which can exhibit Rashba splitting[80]. For this purpose, the term $\left[\left(\frac{1}{2}\right) (\Delta - \alpha_0 \sin(k_y a)) \sigma_x \otimes (\tau_z + \tau_0) + \left(\frac{1}{2}\right) \alpha_0 \sin(k_x a) \sigma_y \otimes (\tau_z + \tau_0)\right]$ (which is the Rashba spin-orbit coupling (RSOC) between the d -electrons) needs to be added to Eq. (8). The coupling can arise in the present system due to proximity of material lacking in the structural inversion symmetry. The Rashba spin-orbit coupling (RSOC) is of particular importance in such semiconductors and the cuprates like Bi2212 as it induces a spin-momentum locking (SML) [81,82]. The SML is a crucial ingredient for several spintronics and topological phenomena [83]. Furthermore, strictly speaking, the Hermiticity of an open system is universally lost, as the system always involves certain degrees of gain and loss. The ubiquitous electron-electron, electron-impurity, and electron-photon scatterings in an electronic system are responsible for this loss/gain. They lead to complex self-energies $\Sigma(k, \omega)$ of single electron states such that the lifetime of a single electron state is always finite. As a consequence, the effective single-particle Hamiltonian of Bloch electron in the periodic potential becomes complex. A fundamental difference between Hermitian and non-Hermitian Hamiltonians is that its linearly independent eigenstates do not span the full Hilbert space. This leads to the possibility that the effective quasiparticle Hamiltonian becomes non-diagonalizable at certain momentum, called “exceptional points”. In two and higher dimensions, the exceptional points are characterized by a nontrivial topological index [84]. There has been a growing interest on this issue [85,86]. These considerations are motivation enough to investigate intensively a non-Hermitian GTKI Hamiltonian.

In conclusion, looking at the controversies and the possibilities, it is anybody’s guess that there are many unsettled issues. Unless other TKI candidates are discovered and thoroughly studied, it

is perhaps difficult to achieve enhancement in the current understanding of strongly correlated topological insulators. In this backdrop, it is pertinent to make an attempt to investigate thoroughly what exactly are the physical explanation of the issues involved. In a future communication we undertake a part of this demanding task.

References

- 1 D. J. Kim, S.Thomas.; T. Grant, J. Botimer, Z. Fisk, J.Xia, Sci. Rep., 3, 3150(2013).
- 2 .M.Dzero, K Sun, V. Galitski, P. Coleman, Phys. Rev. Lett. 2010, 104, 106408(2010); *ibid* Rev. B 2012, 85, 045130 (2012).
- 3.Udai Prakash Tyagi, Kakoli Bera and Partha Goswami, On Strong f -Electron Localization Effect in a Topological Kondo Insulator, *Symmetry*,13(12), 2245 (2021); <https://doi.org/10.3390/sym13122245>.
4. S. Wolgast, C. Kurdak, K. Sun, J. W. Allen, D.-J. Kim, and Z. Fisk, Phys. Rev. B 88, 180405 (2013).
5. X. Zhang, N. P. Butch, P. Syers, S. Ziemak, R. L. Greene, and J. Paglione, Phys. Rev. X 3, 011011 (2013).
6. D. J. Kim, J. Xia, and Z. Fisk, Nat. Mater. 13, 466 (2014).
7. Tran, F.; Blaha, P.,Phys. Rev. Lett. 2009, 102, 226401; A. P. Sakhya and K.B. Maiti , Scientific Reports volume 10, Article number: 1262 (2020).
8. N. Wakeham, P. F. S. Rosa, Y. Q. Wang, M. Kang, Z. Fisk, F. Ronning, and J. D. Thompson, Phys. Rev. B 94, 035127 (2016).
9. P. K. Biswas, M. Legner, G. Balakrishnan, M. C. Hatnean, M. R. Lees, D. M. Paul, E. Pomjakushina, T. Prokscha, A. Suter, T. Neupert, et al., Phys. Rev. B 95, 020410 (2017).
- 10..M. Legner, Topological Kondo insulators: materials at the interface of topology and strong correlations(Doctoral Thesis),ETH Zurich Research Collection(2016).Link:<https://www.research-collection.ethz.ch/bitstream/handle/20.500.11850/155932/eth-49918-02.pdf?isAllowed=y&sequence=2>.
11. A. Sharma, H. Yan, L. Zhang, X.Sun X. B. Liu, Y.Lu Y. Highly enhanced many-body interactions in anisotropic 2D semiconductors. *Accounts of Chemical Research*. 2018;51(5):1164–1173. doi: 10.1021/acs.accounts.7b00504.
- 12.L. Li., W.Han, L. Pi, et al. Emerging in-plane anisotropic two-dimensional materials. *InfoMat*. 2019;1(1):54–73. doi: 10.1002/inf2.12005.
13. . L. Fu and C. L. Kane: Phys. Rev. B 74 195312(2006).
14. S. Sajad Dabiri, Hosein Cheraghchi, Ali Sadeghi, Light-induced topological phases in thin films of magnetically doped topological insulators Physical Review B 103, 205130 (2021); Haowei Xu, Jian Zhou, Ju Li, Light-induced quantum anomalous Hall effect on the 2D surfaces of 3D topological insulators, *Advanced Science*, 2101508 (2021).
15. W. Zhu, M. Umer, and J. Gong, Phys. Rev. Research 3, L032026 (2021).
16. L. Zhou, C. Chen, and J. Gong, Phys. Rev. B 94, 075443 (2016).
17. H. Hubener, M. A. Sentef, U. De Giovannini, A. F. Kemper, and A. Rubio, Nat. Commun. 8, 13940 (2017).
18. D. Zhang, H. Wang, J. Ruan, G. Yao, and H. Zhang, Phys. Rev. B 97, 195139 (2018).

19. H. Liu, J.-T. Sun, and S. Meng, *Phys. Rev. B* **99**, 075121 (2019).
20. L. Li, C. H. Lee, and J. Gong, *Phys. Rev. Lett.* **121**, 036401 (2018).
21. X. Liu, P. Tang, H. Hübener, U. De Giovannini, W. Duan, and A. Rubio, arXiv preprint arXiv:2106.06977 (2021).
22. F. Qin, R. Chen, and H.-Z. Lu, *J. Phys. Condens. Matter* **34**, 225001 (2022).
23. J. W. McIver, B. Schulte, F.-U. Stein, T. Matsuyama, G. Jotzu, G. Meier, and A. Cavalleri, Light-induced anomalous hall effect in graphene, *Nature Physics* **16**, 38 (2019).
24. B. K. Wintersperger, C. Braun, F. N. Unal, A. Eckardt, M. D. Liberto, N. Goldman, I. Bloch, and M. Aidelsburger, Realization of an anomalous floquet topological system with ultracold atoms, *Nature Physics* **16**, 1058 (2020).
25. C. S. Afzal, T. J. Zimmerling, Y. Ren, D. Perron, and V. Van, Realization of anomalous floquet insulators in strongly coupled nanophotonic lattices, *Phys. Rev. Lett.* **124**, 253601 (2020).
26. H. Sambe, Steady states and quasi-energies of a quantum mechanical system in an oscillating field, *Phys. Rev. A* **7**, 2203 (1973).
27. A. A. Pervishko, D. Yudin, and I. A. Shelykh, Impact of high-frequency pumping on anomalous finite-size effects in three-dimensional topological insulators, *Phys. Rev. B* **97**, 075420 (2018).
28. R. Chen, B. Zhou, and D.-H. Xu, Floquet Weyl semimetals in light-irradiated type-II and hybrid line node semimetals, *Phys. Rev. B* **97**, 155152 (2018); R. Chen, D.-H. Xu, and B. Zhou, Floquet topological insulator phase in a Weyl semimetal thin film with disorder, *Phys. Rev. B* **98**, 235159 (2018).
29. N. Goldman and J. Dalibard, Periodically Driven Quantum Systems: Effective Hamiltonians and Engineered Gauge Fields, *Phys. Rev. X* **4**, 031027 (2014); A. Eckardt and E. Anisimovas, High-frequency approximation for periodically driven quantum systems from a Floquet-space perspective, *New J. Phys.* **17**, 093039 (2015).
30. Y. Zhang, C.-X. Liu, X.-L. Qi, X. Dai, Z. Fang, and S.-C. Zhang, Topological insulators in Bi_2Se_3 , Bi_2Te_3 and Sb_2Te_3 with a single Dirac cone on the surface, *Nat. Phys.* **5**, 438 (2009).
31. X.-L. Qi, Y.-S. Wu, and S.-C. Zhang, Topological quantization of the spin hall effect in two-dimensional paramagnetic semiconductors, *Phys. Rev. B* **74**, 085308 (2006).
32. R. Chen, C.-Z. Chen, B. Zhou, and D.-H. Xu, Finite-size effects in non-hermitian topological systems, *Phys. Rev. B* **99**, 155431 (2019).
33. X.-L. Qi and S.-C. Zhang, Topological insulators and superconductors, *Reviews of Modern Physics* **83**, 1057 (2011).
34. Fazekas, P. *Lecture Notes on Electron Correlation and Magnetism*; World Scientific: Singapore, 1999.
35. Peng, C.; Cui, X. Few-body solutions under spin-exchange interaction: Magnetic bound state and the Kondo screening effect. *Phys. Rev. A* **2020**, *102*, 033312.
36. S. Kohler, J. Lehmann, and P. Hänggi, *Phys. Rep.* **406**, 379 (2005).
37. D. Thuberg, E. Muñoz, S. Eggert, and S. A. Reyes, *Phys. Rev. Lett.* **119**, 267701 (2017).
38. G. Stefanucci, S. Kurth, A. Rubio, and E. K. U. Gross, *Phys. Rev. B* **77**, 075339 (2008).
39. B. H. Wu and J. C. Cao, *J. Phys.: Condens. Matter* **20**, 085224 (2008).
40. D. Rai and M. Galperin, *J. Phys. Chem. C* **117**, 13730 (2013).
41. J. Lehmann, S. Kohler, P. Hänggi, and A. Nitzan, *Phys. Rev. Lett.* **88**, 228305 (2002).
42. B. H. Wu and C. Timm, *Phys. Rev. B* **81**, 075309 (2010).
43. B. H. Wu and J. C. Cao, *Phys. Rev. B* **73**, 245412 (2006).
44. N. Tsuji, T. Oka, and H. Aoki, *Phys. Rev. B* **78**, 235124 (2008).
45. B. H. Wu and J. C. Cao, *Phys. Rev. B* **81**, 085327 (2010).

46. G. Li et al., *Science*, 346, 1208–1212(2014). This study is the first report of the quantum oscillations in magnetization in Kondo insulators.

47. B.S.Tan, Y.T.Hsu, B.Zeng, M.C. Hatnean, N. Harrison, Z. Zhu, M. Hartstein, M. Kiourlappou, A. Srivastava, M. D. Johannes, et al. Unconventional Fermi surface in an insulating state. *Science*, 349, 287–290(2015).

48. M. Hartstein, W.H.Toews, Y.T. Hsu, B. Zeng, X. Chen, M.C. Hatnean, Q.R. Zhang, S. Nakamura, A.S. Padgett, G.Rodway-Gant, et al.,*Nat. Phys.* 14, 166–172(2018).

49. Flachbart, K.; Gabáni, S.; Neumaier, K.; Paderno, Y.; Pávlík, V.; Schuberth, E.; Shitsevalova, N. Specific heat of SmB₆ at very low temperatures. *Physica. B* 378, 610–611(2006).

50. G. Baskaran, arXiv: 1507.03477 v1 (2015)

51. Knolle, J. & Cooper, N. R., *Phys. Rev. Lett.* 118, 096604 (2017).

52. Erten, O., Chang, P.-Y., Coleman, P. & Tsvetlik, A. M., *Phys. Rev. Lett.* 119, 057603 (2017).

53. Chowdhury, D., Sodemann, I. & Senthil, T., *Nat. Commn.* 9, 1766 (2018).

54. Sodemann, I., Chowdhury, D. & Senthil, T., *Phys. Rev. B* 97, 045152 (2018).

55. Shen, H. and Fu, L., *Phys. Rev. Lett.* 121, 026403 (2018).

56. Z. Xiang, Y. Kasahara, T. Asaba, B. Lawson, C. Insman, Lu Chen, K. Sugimoto, S. Kawaguchi, Y. Sato, G. Li, S. Yao, Y.L. Chen, F. Iga, J. Singleton, Y. Matsuda, and L. Li, *Science* 69, 65 (2018).

57. P. G. LaBarre et al., arXiv:2204.05392v1 (2022), To be published in JPCM.

58. M. Orendáč, S. Gabáni, G. Pristáň, E. Gažo, P. Diko, P. Farkašovský, A. Levchenko, N. Shitsevalova and K. Flachbart, “Isosbestic Points in Doped SmB₆ as features of Universality and Property Tuning”, *Phys. Rev. B*, 96, 115101 (2017).

59. J. Stankiewicz, M. Evangelisti, P.F.S. Rosa, P. Schlottmann and Z. Fisk, “Physical Properties of SmxB₆ Single Crystals”, *Phys. Rev. B*, 99, 045138 (2019).

60. Fuhrman, W.T., Chamorro, J.R., Alekseev, P. *et al.* Screened moments and extrinsic in-gap states in samarium hexaboride. *Nat Commun* 9, 1539 (2018). <https://doi.org/10.1038/s41467-018-04007-z>

61. In fact, we have the literature where it is reported that the material may show a linear T-term in the specific heat which has a coefficient that varies between 2 and 25 mJ/mole/K², depending upon the sample preparation [7, 16, 17]. Doping with 5% of magnetic impurities can lead to an order of magnitude increase in the heat capacity [18].

62. Z.Xiang et al., *Science* 362, 65-69 (2018).

63. Y. Sato et al., *Nat. Phys.* 15, 954 (2019).

64. M. E. Boulanger et al., *Phys. Rev. B.* 97, 245141 (2018).

65. Y. Xu et al., *Phys. Rev. Lett.* 116, 246403 (2016).

66. S. Sen et al., *Physical Review Research* 2, 033370 (2020).

67. P F S Rosa and Z Fisk, *Bulk and Surface Properties of SmB₆ Rare-Earth Borides*, ed Inosov D S (New York: Jenny Stanford Publishing) chap 11(2021).

68. Kasuya, T., Takegahara, K., Fujita, T., Tanaka, T. and Bannai, E. Valence fluctuating state in SmB₆. *J. Phys. Colloq.* 40, C5–308 (1979).

69. M. Orendáč, et al. Isosbestic points in doped SmB_6 as features of universality and property tuning. *Phys. Rev. B* **96**, 115101 (2017).
70. W. Phelan et al., Correlation between bulk thermodynamic measurements and the low-temperature-resistance plateau in SmB_6 . *Phys. Rev. X* **4**, 031012 (2014).
71. Riseborough, P. S. Collapse of the coherence gap in Kondo semiconductors. *Phys. Rev. B* **68**, 235213 (2003).
72. Gabáni, S. et al. Magnetic properties of SmB_6 and $\text{Sm}_{1-x}\text{La}_x\text{B}_6$ solid solutions. *Czechoslov. J. Phys.* **52**, A225–A228 (2002).
73. M. Abele, X. Yuan, and P. S. Riseborough, *Phys. Rev. B* **101**, 094101 – Published 2 March 2020.
74. R. Sollie and P. Schlottmann, “A Simple Theory of the Kondo Hole”, *J. Appl. Phys.* **69**, 5478-5480 (1991).
75. M.E. Valentine, S. Koohpayeh, W.A. Phelan, T.M. McQueen, P.F.S. Rosa, Z. Fisk and N. Drichko, “Breakdown of the Kondo Insulating State in SmB_6 by introducing Sm Vacancies”, *Phys. Rev. B*, **94**, 075102 (2016).
76. P.S. Riseborough, “Collapse of the Coherence Gap in Kondo Semiconductors”, *Phys. Rev. B*, **68**, 235213 (2003).
77. N.J. Laurita, C.M. Morris, S.M. Koohpayeh, P.F.S. Rosa, W.A. Phelan, Z. Fisk, T.M. McQueen and N.P. Armitage, “Anomalous Three-Dimensional Bulk ac Conduction within the Kondo Gap of SmB_6 Single Crystals”, *Phys. Rev. B*, **94**, 165154 (2016).
78. N. Xu, P.K. Biswas, J.H. Dil, R.S. Dhaka, G. Landolt, S. Muff, C.E. Matt, X. Shi, N.C. Plumb, M. Radović, E. Pomjakushina, K. Conder, A. Amato, S.V. Borisenko, R. Yu, H.-M. Weng, Z. Fang, X. Dai, J. Mesot, H. Ding, M. Shi, *Nat. Commun.* **5**, 4566 (2014).
79. S. Suga et al., *J. Phys. Soc. Jpn* **83**, 014705 (2014).
80. Hlawenka, P., Siemensmeyer, K., Weschke, E. *et al.* Samarium hexaboride is a trivial surface conductor. *Nat Commun* **9**, 517 (2018). <https://doi.org/10.1038/s41467-018-02908-7>
81. R. Winkler. Spin–Orbit Coupling Effects in Two-Dimensional Electron and Hole Systems, 2003, Volume 191, ISBN : 978-3-540-01187-3.
82. J. Chen, K. Wu, W. Hu, and J. Yang, Spin–orbit coupling in 2d semiconductors: A theoretical perspective, *J. Phys. Chem. Lett.* **12**, 12256 (2021).
83. A. Manchon, H. C. Koo, J. Nitta, S. M. Frolov, and R. A. Duine, New perspectives for rashba spin–orbit coupling, *Nat. Mater.* **871**(2015).
84. H. Eleuch and I. Rotter, *Phys. Rev. A* **95**, 022117 (2017).
85. Bo Zhen, Chia Wei Hsu, Yuichi Igarashi, Ling Lu, Ido Kaminer, Adi Pick, Song-Liang Chua, John D. Joannopoulos and Marin Soljacic, *Nature*, **525**, 354(2015).
86. M. Dzero, J. Xia, V. Galitski, and P. Coleman, *Annual Review of Condensed Matter Physics*, **7**, 249 (2016).

Appendix A

Eigenvalues and eigenvectors of the matrix in Eq.(8): The functions appearing in Eq. (8) are given as below:

$$A_1 = 2Vb, \mathbf{k} = (k_x, k_y), k^2 = (k_x^2 + k_y^2),$$

$$\epsilon(k, q, \mu, b) = \epsilon_0(\mu, b) - D_1(b)a^2q^2 + D_2(b)a^2k^2 + O(a^4q^4) + O(a^4k^4)$$

$$\vartheta(k, q, b) = \vartheta_0(b) - B_1(b)a^2q^2 + B_2(b)a^2k^2 + O(a^4q^4) + O(a^4k^4)$$

$$\epsilon_0(\mu, b) = -\mu + \left[\frac{b^2}{2} \epsilon_f - 3t_{d1} - 3t_{f1} - 6t_{d2} - 6t_{f2}b^2 - 4t_{d3} - 4t_{f3}b^2 \right],$$

$$D_1(b) = D_2(b) = \left[\frac{t_{d1} + b^2 t_{f1}}{2} + 2(t_{d2} + b^2 t_{f2}) + 2(t_{d3} + b^2 t_{f3}) \right],$$

$$\vartheta_0(b) = \left[-\frac{b^2 \epsilon_f}{2} - 6t_{d2} + 6t_{f2}b^2 - 4t_{d3} + 4t_{f3}b^2 \right],$$

$$B_1(b) = B_2(b) = \left[\frac{t_{d1} - b^2 t_{f1}}{2} + 2(t_{d2} - b^2 t_{f2}) + 2(t_{d3} - b^2 t_{f3}) \right]. \quad (\text{A.1})$$

There are terms of $O(a^4 q^4)$, $O(a^4 k^4)$, and higher in the Hamiltonian (8) which have not been taken into account for the graphics, etc. above. The eigenvalues of the matrix in Eq.(8) are given by the quartic $\epsilon_j^4 + a \epsilon_j^3 + b \epsilon_j^2 + c \epsilon_j + d = 0$ in Eq.(13). The coefficients (a, b, c, d) of the quartic are given by

$$a = -2(\epsilon_d + \epsilon_c), \epsilon_d = (\epsilon(k, q, \mu, b) + \vartheta(k, q, b)), \epsilon_c = (\epsilon(k, q, \mu, b) - \vartheta(k, q, b)), \quad (\text{A.2})$$

$$b = (AB + CD) + 4\epsilon_d \epsilon_c + \epsilon_c^2 + 2(d_1^2 + d_2^2 + d_3^2), \quad (\text{A.3})$$

$$c = -2(\epsilon_c AB + \epsilon_d CD + (\epsilon_d + \epsilon_c)(d_1^2 + d_2^2 + d_3^2)), \quad (\text{A.4})$$

$$d = [ABCD + (AD + BC)((d_1^2 + d_2^2) + (AC + BD)d_3^2 + (d_1^2 + d_2^2 + d_3^2)^2], \quad (\text{A.5})$$

$$A = (\epsilon_d + M), B = (\epsilon_d - M), C = (\epsilon_c + M), D = (\epsilon_c - M). \quad (\text{A.6})$$

The following symbols are defined in the main text: $ak_{\mp} = ak_x \mp iak_y$, $d_0 = \frac{\epsilon_d - \epsilon_c}{2}$, $d_1 = -iA_1 ak_y$, $d_2 = iA_1 ak_x$, $d_3 = A_1 a\chi$, and the hybridization parameter $A_1 = 2Vb$. The functions appearing in Eq. (14) are given by

$$\begin{aligned} \eta_0(k) &= \frac{2b_0(k)}{3} + (\Delta(k) - \Delta_0(k))^{\frac{1}{3}} - (\Delta(k) + \Delta_0(k))^{\frac{1}{3}}, \quad \Delta_0(k) = \left(\frac{b_0^3(k)}{27} - \frac{b_0(k)d_0(k)}{3} - c_0^2(k) \right), \\ \Delta(k) &= \left(\frac{2}{729} b_0^6 + \frac{4d_0^2 b_0^2}{27} + c_0^4 - \frac{d_0 b_0^4}{81} - \frac{2b_0^3}{27} + \frac{2c_0^2 b_0 d_0}{3} + \frac{d_0^3}{27} \right)^{1/2}, \quad b_0(k) = \left\{ \frac{3a^2 - 8b}{16} \right\}, \\ c_0(k) &= \left\{ \frac{-a^3 + 4ab - 8c}{32} \right\}, \quad d_0(k) = \frac{-3a^4 + 256d - 64ac + 16a^2 b}{256}. \end{aligned} \quad (\text{A.7})$$

As regards the eigenstates linked to the eigenvalues in ϵ_j ($s, \sigma, k, q, \mu, b, M$) in (13), these Bloch states are given by

$$|\psi^{(j)}(k)\rangle = \begin{pmatrix} \psi_1^j(k) \\ \psi_2^j(k) \\ \psi_3^j(k) \\ \psi_4^j(k) \end{pmatrix}, \quad j=1, 2, 3, 4, \quad (\text{A.8})$$

$$\begin{aligned}\psi_1^j(k) &= g_1^j(k), \quad \psi_2^j(k) = (-iak_+) f_2^j(k) g_1^j(k), \quad \psi_3^j(k) = i(\epsilon_j - \epsilon_d + M) f_3^j(k) g_1^j(k), \\ \psi_4^j(k) &= (-A_1 a k_+) f_4^j(k) g_1^j(k),\end{aligned}\tag{A.9}$$

$$\begin{aligned}g_1^j(k) &= \Upsilon_j^{-1/2}(k) = (1 + a^2 k^2 |f_2^j(k)|^2 + (\epsilon_j - \epsilon_d + M)^2 |f_3^j(k)|^2 + A_1^2 a^2 k^2 |f_4^j(k)|^2)^{-\frac{1}{2}}, \\ f_2^j(k) &= (aq)^{-1} [(\epsilon_j - \epsilon_d - M)(\epsilon_j - \epsilon_c + M) + A_1^2 a^2 k^2 + A_1^2 a^2 q^2] \times [(\epsilon_j - \epsilon_d + \\ &M)(\epsilon_j - \epsilon_c + M) + A_1^2 a^2 k^2 + A_1^2 a^2 q^2]^{-1}\end{aligned}\tag{A.10}$$

$$\begin{aligned}f_3^j(k) &= (A_1 a q)^{-1} [(\epsilon_j - \epsilon_d - M)(\epsilon_j - \epsilon_c + M) + A_1^2 a^2 k^2 + \eta A_1^2 a^2 q^2] \\ &\times [(\epsilon_j - \epsilon_d + M)(\epsilon_j - \epsilon_c + M) + A_1^2 a^2 k^2 + A_1^2 a^2 q^2]^{-1}, \quad \eta = \frac{(\epsilon_j - \epsilon_d - M)}{(\epsilon_j - \epsilon_d + M)},\end{aligned}\tag{A.11}$$

$$f_4^j(k) = 2M / [(\epsilon_j - \epsilon_d + M)(\epsilon_j - \epsilon_c + M) + A_1^2 a^2 k^2 + A_1^2 a^2 q^2].\tag{A.12}$$

Here $\epsilon_j = \epsilon_j(s, \sigma, k, b, M)$ is given by Eq. (14). In the special case $M \rightarrow 0$, $\psi_1^j(k) = \Upsilon_j^{-1/2}(k)$, $\psi_2^j(k) = \frac{d_1 + id_2}{d_3} \Upsilon_j^{-1/2}(k)$, $\psi_3^j(k) = \frac{(\epsilon_j - \epsilon_d)}{d_3} \Upsilon_j^{-1/2}(k)$, and $\psi_4^j(k) = 0$. We find that the function $\Upsilon_j^{-1/2}(k)$ is given by $\frac{aq}{\left[\frac{(\epsilon_j - \epsilon_d)^2}{A_1^2} + (ak)^2 + (aq)^2\right]^{1/2}}$. The eigenvectors in this special case are

$$|\acute{u}^{(j)}(k)\rangle = \begin{pmatrix} \frac{aq}{\left[\frac{(\epsilon_j - \epsilon_d)^2}{A_1^2} + (ak)^2 + (aq)^2\right]^{1/2}} \\ -iak_+ \\ \frac{(\epsilon_j - \epsilon_d)}{A_1} \\ 0 \end{pmatrix}.\tag{A.13}$$

Z₂ invariant of the system: We wish to calculate the Z₂ invariant of the system in order to show that SmB₆ is indeed a strong TI. We feel necessary to outline the method [13] in an effort to make the present communication comprehensive. We consider the green and red bands in Figure 2(a), and denote their Bloch wave functions, respectively, as $|\acute{u}^{(1)}(k)\rangle$ and $|\acute{u}^{(2)}(k)\rangle$ for this purpose, where following Fu and Kane[13] we assume the system one dimensional, i.e. $\mathbf{k} = (k, 0)$. We impart the time dependence assuming that the band parameters change with time and return to the original values at $t = T$. We also suppose that the Hamiltonian $h_{\text{surface}}^{BHZ}(M = 0)$ satisfies the following

conditions $h_{\text{surface}}^{\text{BHZ}}(M=0, -t) = \Theta h_{\text{surface}}^{\text{BHZ}}(M=0, t) \Theta^{-1}$ and $h_{\text{surface}}^{\text{BHZ}}(M=0, t+T) = h_{\text{surface}}^{\text{BHZ}}(M=0, t)$. It is well-known [13] that charge polarization P can be calculated by integrating the Berry connection of the occupied states over the BZ. In the present case of the two-band system, P may be written as $P = P_1 + P_2$ where the Berry connections $\{-i\langle \dot{u}^{(\alpha)}(\mathbf{k}) | \nabla_{\mathbf{k}} | \dot{u}^{(\alpha)}(\mathbf{k}) \rangle\}$ are given by $c_{\alpha\alpha}(k)$ ($\alpha = 1, 2$) and $P_1 = \int_{-\pi}^{\pi} \frac{dk}{2\pi} c_{11}(k)$, $P_2 = \int_{-\pi}^{\pi} \frac{dk}{2\pi} c_{22}(k)$. The Berry curvature is given by $\Omega_{\alpha}(k) = \nabla_{\mathbf{k}} \times c_{\alpha\alpha}(k)$. The total polarization density $C(k) = c_{11}(k) + c_{22}(k)$. This yields the TR polarization which is defined by $P_{tr} = P_1 - P_2 = 2P_1 - P$. Here P_{tr} gives the difference in charge polarization between spin-up and spin-down quasiparticle bands. We now go back the charge polarization P , calculated by integrating the Berry connection of the occupied states over the BZ. Furthermore, the time-reversed version of $|\dot{u}^{(2)}(\mathbf{k})\rangle$ is equal to $|\dot{u}^{(1)}(-\mathbf{k})\rangle$ except for a phase factor. Hence, at $t = 0$ and $t = T/2$ one may write $\Theta |\dot{u}^{(2)}(\mathbf{k})\rangle = e^{-i\rho(k)} |\dot{u}^{(1)}(-\mathbf{k})\rangle$ and $\Theta |\dot{u}^{(1)}(\mathbf{k})\rangle = -e^{-i\rho(-k)} |\dot{u}^{(2)}(-\mathbf{k})\rangle$. It is not difficult to see that the matrix representation of the TR operator Θ in the Bloch wave function basis $\xi_{\alpha\beta}(k) \equiv \{\langle \dot{u}^{(\alpha)}(-\mathbf{k}) | \Theta | \dot{u}^{(\beta)}(\mathbf{k}) \rangle\}$ will now be given as $\xi(k) = \begin{pmatrix} 0 & e^{-i(k)} \\ -e^{-i\rho(k)} & 0 \end{pmatrix}$. One can easily confirm that $\xi_{\alpha\beta}(k)$ is a unitary matrix. It has the property $\xi_{\alpha\beta}(-k) = -\xi_{\alpha\beta}(k)$. This implies that $\xi_{\alpha\beta}(k)$ is anti-symmetric at a TRIM. Upon getting back to the connections, we note that the connections satisfy $c_{11}(-k) = c_{22}(k) - \frac{\partial}{\partial k} \rho(k)$. These lead us to the charge polarization between spin-up bands P_1 as $P_1 = \int_0^{\pi} \frac{dk}{2\pi} C(k) - \frac{i}{2\pi} [\rho(\pi) - \rho(0)]$. Since $\rho(k) = i \log \xi_{12}(k)$, and $C(k) = \text{tr}(c(k))$, after a little algebra, we find

$$P_{tr} = \frac{1}{i\pi} \log \left(\frac{\sqrt{\xi_{12}(0)^2}}{\xi_{12}(0)} \cdot \frac{\xi_{12}(\pi)}{\sqrt{\xi_{12}(\pi)^2}} \right). \quad (\text{A.14})$$

Obviously enough, the argument of the logarithm is $+1$ or -1 . Furthermore, since $\log(-1) = i\pi$ one can see that P_{tr} is 0 or 1 (mod 2). Physically, of course, the two values of P_{tr} corresponds to two different polarization states which the system can take at $t = 0$ and $t = T/2$. The Bloch functions $|\dot{u}^{(\alpha)}(k, t)\rangle$ introduced above could be visualized as maps from the 2D phase space (k, t) to the Hilbert space. As in refs.[13], the Hilbert space could be separated into two parts depending on the difference in P_{tr} between $t = 0$ and $t = T/2$. This leads to introduction of a quantity ν_0 , specified only in mod 2, and defined as $(P_{tr}(\frac{T}{2}) - P_{tr}(0))$: When P_{tr} does not changes between $t = 0$ to $T/2$, $\nu_0 = 0$, whereas if there is a change then $\nu_0 = 1$. The visualization mentioned above, thus, yields that the Hilbert space is trivial if $\nu_0 = 0$, while for $\nu_0 = 1$ it is nontrivial (twisted). Equivalently, the system band structures are characterized by Kane–Mele index [73] $Z_2 = +1$ ($\nu_0 = 0$) and $Z_2 = -1$ ($\nu_0 = 1$). We obtain $(-1)^{\nu_0} = \prod_j \frac{\xi_{12}(k_{\text{trim}}^{(j)})}{\sqrt{\xi_{12}(k_{\text{trim}}^{(j)})^2}}$. We now consider the generalization of this result.

For this purpose, we suppose that $2N$ bands are occupied and forming N Kramers pairs. For each

such pair n , at the TR symmetric times $t = 0$ and π the wave functions are related by write $\Theta|\psi_n^{(2)}(\mathbf{k})\rangle = e^{-i\rho_n(k)}|\psi_n^{(1)}(-\mathbf{k})\rangle$ and $\Theta|\psi_n^{(1)}(\mathbf{k})\rangle = e^{-i\rho_n(k)}|\psi_n^{(2)}(-\mathbf{k})\rangle$ and the matrix $\xi(k) =$

$$\begin{pmatrix} 0 & e^{-i\rho_1(k)} & 0 & 0 & \dots \\ -e^{-i\rho_1(-k)} & 0 & 0 & 0 & \dots \\ 0 & 0 & 0 & e^{-i\rho_2(k)} & \dots \\ 0 & 0 & -e^{-i\rho_2(-k)} & 0 & \dots \\ \vdots & \vdots & \vdots & \vdots & \ddots \end{pmatrix}. \quad (\text{A.15})$$

This leads to $\xi_{12}(\mathbf{k}_{\text{trim}}^{(j)}) \xi_{34}(\mathbf{k}_{\text{trim}}^{(j)}) \dots \dots \dots \xi_{2N-1, 2N}(\mathbf{k}_{\text{trim}}^{(j)}) = e^{-i\sum_{n=1}^N \rho_n(\mathbf{k}_{\text{trim}}^{(j)})} = \text{Pf}[\xi(\mathbf{k}_{\text{trim}}^{(j)})]$, where Pfaffian is defined for an antisymmetric matrix and is related to the determinant by $\text{Pf}[A]^2 = \det[A]$. The counter-part of Eq.(A.14), in this general case, is given by $P_{tr} = \frac{1}{i\pi} \log\left(\frac{\sqrt{\det[\xi(0)]}}{\text{Pf}[\xi(0)]} \cdot \frac{\text{Pf}[\xi(\pi)]}{\sqrt{\det[\xi(0)]}}\right)$. Thus, the Z_2 topological invariant ν is given by $(-1)^\nu = \prod_j \delta(\mathbf{k}_{\text{trim}}^{(j)})$ where for each TRIM $\mathbf{k}_{\text{trim}}^{(j)}$ one defines

$$\delta(\mathbf{k}_{\text{trim}}^{(j)}) \equiv \frac{\text{Pf}[\xi(\mathbf{k}_{\text{trim}}^{(j)})]}{\sqrt{\det[\xi(\mathbf{k}_{\text{trim}}^{(j)})]}}. \quad (\text{A.16})$$

As we will see in the main text, this leads to the classification of the Hilbert space into the twisted ($\nu=1$) and the trivial one ($\nu=0$).